


# Band structure properties, phonons, and exciton fine structure in 4H-SiC measured by wavelength-modulated absorption and low-temperature photoluminescence

W. M. Klahold<sup>✉,\*</sup>, W. J. Choyke<sup>✉,†</sup> and R. P. Devaty<sup>✉,‡</sup>

Department of Physics and Astronomy, University of Pittsburgh, 3941 O'Hara Street, Pittsburgh, Pennsylvania 15260, USA

 (Received 17 July 2020; revised 21 October 2020; accepted 22 October 2020; published 23 November 2020)

Owing to its hexagonal symmetry, indirect band gap, and relatively large unit cell, the electronic band structure of 4H-SiC is comprised of a complicated series of anisotropic valence and conduction band extrema even very near to the uppermost valence band maximum and lowest conduction band minimum. This has presented a difficult challenge to those experiments which have attempted to resolve the small energy separations between these band extrema. To overcome this challenge, we have measured the wavelength-modulated absorption (WMA) spectrum of 4H-SiC over a broader wavelength range (3500–3800 Å) and at a higher resolution ( $<0.1$  Å) than in previous work. By comparing these measurements with the low-temperature photoluminescence spectrum in ultrapure 4H-SiC, we have identified several features, which we attribute to a  $56 \pm 3$  meV crystal-field splitting of the valence band maximum or a  $136 \pm 3$  meV separation between the two lowest conduction band minima. We also show that the spin-orbit split-off valence band, which has been observed in previous measurements of 4H-SiC, contributes to nonparabolic dispersion near the valence band maximum, and this is responsible for several previously misidentified features in the WMA spectrum. Finally, we report the first experimental measurement of fine structure splittings in the free exciton ground state, which manifests as four small ( $0.7 \pm 0.1$  meV) splittings in the WMA spectrum due to mass anisotropy and electron-hole exchange interaction.

DOI: [10.1103/PhysRevB.102.205203](https://doi.org/10.1103/PhysRevB.102.205203)

## I. INTRODUCTION

While the first measurements of the fundamental absorption edge in silicon carbide were published by Weigel in 1915 [1], it was not until the late 1950s and 1960s that the fundamental absorption edge of several different polytypes of SiC was measured and also interpreted in terms of phonon-assisted transitions of electrons across the fundamental energy gap [2–8]. These studies came at an opportune time due not only to the recent advancements in the quantum theory of light absorption in semiconductors and insulators [9] but also to the newly developed Lely method [10] for growth of high-purity SiC crystals. As a result, this work produced some of the first experimental insights into the size, temperature dependence, and indirect nature of the band gaps of several polytypes of SiC as well as the energies of the principal momentum-conserving phonons involved in exciting electrons across the indirect gaps.

In the time since these experimental results were published, there have been a great many calculations of the electronic band structure [11–18] and phonon dispersion [18–24] using either *ab initio* or semiempirical methods. Aside from the well-known underestimation of the band gap typical of earlier density functional theory (DFT) calculations under the local density approximation, the gross features of these calculations

show good agreement with each other and with experiments, although there remains some divergence in the finer details. In general, these calculations show that, for the 4H polytype of SiC, the uppermost valence band maximum and the lowest conduction band minimum both lie within a few 0.1 eV of one or more additional band extrema. The precise energy separations between the extrema are usually small compared to the indirect gap, although they may vary by as much as a factor of three in the literature.

In this work, we focus on the three highest valence band maxima and the two lowest conduction band minima. The three highest valence band maxima are each at or very near to the  $\Gamma$  point of the Brillouin zone, where they are each twofold degenerate (including spin) (see Fig. 1). We refer to the splitting between the two highest maxima as the spin-orbit splitting  $\Delta_{so}$ , and to the splitting between the highest and third highest maxima as the crystal-field splitting  $\Delta_{cf}$ . The latter splitting refers to the effect of the hexagonal crystal environment breaking the threefold degeneracy of the *p*-like orbital states associated with the valence band maximum. The two lowest conduction band minima are each twofold degenerate (including spin) at or very near to the *M* point of the Brillouin zone. We refer to the energy splitting between these two minima simply as the conduction band splitting  $\Delta_{c2}$ . We note, however, that  $\Delta_{c2}$  appears not to be a splitting in the sense of a broken degeneracy, but originates from the folding of the lowest conduction band in 2H-SiC along the *M-U-L* line. In particular, the lowest conduction band minimum in 4H-SiC appears to originate from the conduction band at *M* in 2H-SiC, and the second lowest conduction band minimum

\*ashwmk@gmail.com

†choyke@pitt.edu

‡devaty@pitt.edu

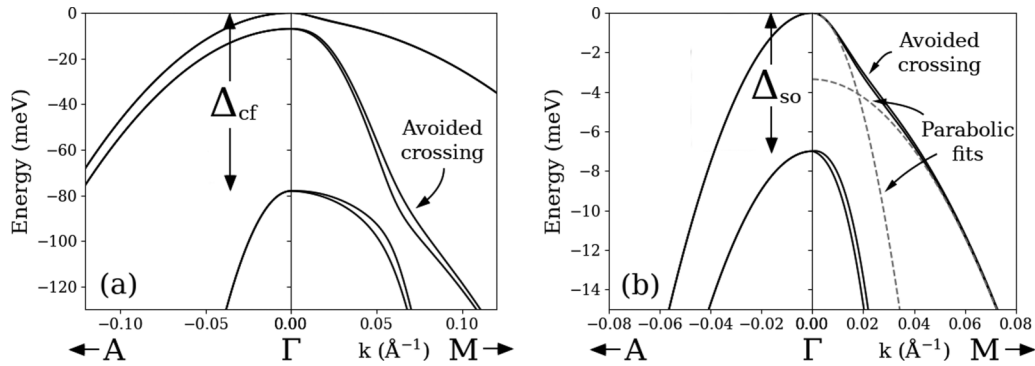


FIG. 1. (a) Three highest valence band maxima and (b) close-up view of the two highest maxima, plotting using the  $\vec{k} \cdot \vec{p}$  band parameters of Wellenhofer and Rössler [14]. Each maximum is twofold degenerate including spin, and the degeneracy breaks along directions perpendicular to  $\Gamma$ -A.  $\Delta_{so}$  and  $\Delta_{cf}$  denote, respectively, the spin-orbit and crystal-field splittings of the valence band maximum. Avoided crossings between pairs of energy bands are marked by arrows. Dashed lines show parabolic fits to the topmost valence band maximum on either side of the avoided crossing.

in 4H-SiC appears to originate from the conduction band at L in 2H-SiC (see Fig. 7 of Ref. [15]).

While the scales of these energy separations may be comparable to the accuracy of the band structure calculations, they are nevertheless of considerable relevance to the modeling of high-temperature devices [25], high-field carrier transport [26–28], and shallow donor levels [29]. Despite this fact, there exist, even today, only a few experimental estimates for these parameters, which in some cases show appreciable variance among the different methods used. As a result, the aforementioned models have either had to neglect these parameters or rely upon their calculated values. Perhaps the most direct measurements come from recent wavelength-modulated absorption (WMA) [30,31] and free carrier absorption (FCA) [32,33] measurements of 4H-SiC, which identified spectral features associated with indirect transitions between each of the three uppermost valence band maxima and the two lowest conduction band minima. In these measurements, the spin-orbit splitting was readily observed, and there is good agreement between its measured value and that calculated in the relativistic band structure calculations of Persson and Lindelfelt [16] and Lyu and Lambrecht [34]. However, only a few spectrally broad features have been observed and attributed to the splittings  $\Delta_{cf}$  and  $\Delta_{c2}$ , which impedes an unambiguous identification of the participating momentum-conserving phonons and the energetic position of the corresponding band extrema.

Electroabsorption [35], ballistic electron/hole emission microscopy (BEEM/BHEM) [36–38], and surface photovoltage spectroscopy (SPS) [39] have also been used to measure the relative energy separations of these band extrema, although, for these experiments, the need to probe samples through use of Schottky or metal-insulator-semiconductor contacts makes interpretation of results somewhat less straightforward than the aforementioned WMA and FCA techniques. In any case, the experimental signatures for  $\Delta_{cf}$  and  $\Delta_{c2}$  are weak in comparison with those associated with the transitions between the two highest valence band maxima and the lowest conduction band minimum.

Initially, it was supposed that this could be the result of poor sample quality. Therefore, motivated by the recent

progress in growth of high-quality 4H-SiC, we undertook to measure the WMA spectrum of high-purity boules and free-standing epilayers of 4H-SiC over a broader spectral range of the near band edge and at higher wavelength resolution than has previously been attempted. Although the boules samples contained approximately two orders of magnitude higher impurity concentration ( $\sim 10^{15} \text{ cm}^{-3}$  nitrogen) than that of the free-standing epilayers, the WMA spectra of both groups of samples were found to be consistent with each other and were comprised of the spectral signatures of free indirect excitons, and so we consider both on equal terms in our examination of the fundamental gap in 4H-SiC. By supplementing these measurements with low-temperature photoluminescence (LTPL) measurements of the same boules and epilayer samples, we have identified two groups of spectral features in the WMA spectrum which are reliably reproduced in all samples studied and can be assigned to indirect transitions associated with the crystal-field splitting  $\Delta_{cf}$  and conduction band splitting  $\Delta_{c2}$ . Interestingly, the spectral widths of these features did not vary over the wide range of samples (including both boules and epitaxial material) and remained comparable to those observed in previous WMA measurements of 4H-SiC [30,31]. From this, we infer that the spectral broadening is intrinsic in nature and is probably due to the reduced lifetime for the associated excitons relative to those associated with more closely spaced valence and conduction band extrema.

We also wish to highlight several new features of the fundamental absorption edge of 4H-SiC which in previous studies were misidentified, overlooked, or not observed due to insufficient spectral resolution. We first consider several pairs of features split by the spin-orbit splitting of the valence band which also exhibit a much broader feature lying in between, which we attribute to an avoided crossing between the topmost valence band and the second lowest, spin-orbit split-off valence band. Secondly, we discuss a series of small,  $\sim 0.7$  meV splittings observed in the indirect absorption onsets due to several different phonons which we attribute to electron mass anisotropy and exchange-related splittings in the ground state of the free exciton. The size of these splittings is comparable to mass anisotropy and exchange-related splittings in other indirect semiconductors

(including 3C-SiC) [40–46], and we show using group theory that the multiplicity and polarization dependence of the splittings are consistent with this identification.

These results are the culmination of all of our recent high-resolution WMA and LTPL measurements of 4H-SiC, which encompass, expand upon, or revise those described in two of our brief conference reports, the first of which reported on evidence for the conduction band splitting  $\Delta_{c2}$  [31] and the second of which described those features due to the avoided crossing in the valence band or to mass anisotropy and exchange splittings [47]. As will be described below in Sec. III, our preliminary result for  $\Delta_{c2}$  was subject to a non-negligible systematic error which, in the present paper, we have eliminated by fitting the WMA spectra to an appropriate model function [48–50]. For the same reason, our result for the crystal-field splitting  $\Delta_{cf}$ , which has not been previously published for the sample set used in this study, is similarly improved over past WMA measurements of 4H-SiC. Our assignments of certain spectral features to an avoided crossing in the valence band remain the same as they were in our previous report [47]. However, here we provide a direct comparison between these features and the calculated valence band density of states (more specifically, its derivative), which bolsters the assignments significantly. Finally, regarding the series of small,  $\sim 0.7$  meV splittings, we have identified an additional  $\sim 0.7$  meV splitting in a relatively weak absorption onset which was not reported previously. Here we also give a more complete description of our group theory arguments which validate our assignment of these splittings to mass anisotropy and exchange splittings in the free exciton ground state. We also report an interesting correlation between the sizes of the observed spin-orbit splittings in the WMA spectrum and the symmetries of the associated momentum-conserving phonons. This will be shown to provide further support to our identification of the ground state splittings of the free exciton. To our knowledge, this is the first time this correlation has been reported.

## II. EXPERIMENT

The apparatus used for measuring the WMA spectrum (shown in Fig. 2) has been described previously [30,47], and is based on a scheme proposed by Shaklee and Rowe [50]. In brief, it consists of a 1000-W xenon arc lamp and SPEX 1401 double monochromator, which together are used to generate a monochromatic beam that is then collimated and directed at normal incidence onto a sample. A Glan-Thompson prism is used to linearly polarize the incident beam either parallel or perpendicular to the sample's  $c$  axis, and the intensity of the transmitted beam is measured using a photomultiplier tube. Throughout the course of a measurement, the beam is simultaneously chopped (at a frequency  $f_c = 217$  Hz) by a chopper wheel placed just outside the monochromator exit slit and wavelength modulated. Wavelength modulation is achieved with a 3-mm-thick fused silica plate just inside the monochromator entrance slit. Using an amplitude-stabilized driver, the plate is made to vibrate torsionally (at frequency  $f_\lambda = 75$  Hz) about an axis normal to the monochromator's plane of dispersion, scanning the entrance slit image back and forth across the exit slit and varying the wavelength

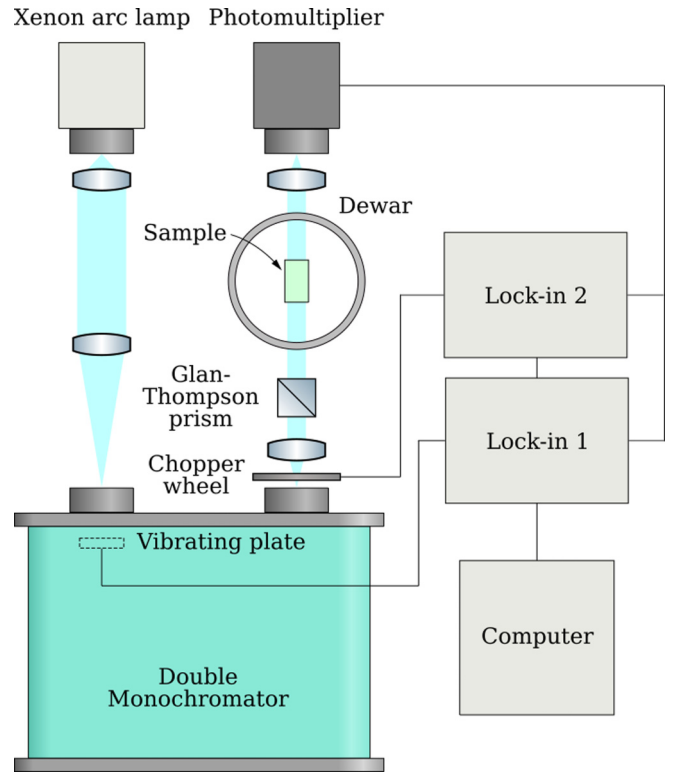


FIG. 2. Apparatus for wavelength-modulated absorption measurements. The vibrating fused silica plate oscillates torsionally about an axis normal to the page, sweeping the entrance slit image back and forth across the exit slit to achieve wavelength modulation.

by an amount  $\Delta\lambda$  about a mean wavelength  $\lambda_o$ . Due to the wavelength dependence of the light transmitted through the sample, there is an AC ripple in the transmitted intensity with amplitude

$$\Delta I = \frac{dI}{d\lambda} \Delta\lambda. \quad (1)$$

A pair of lock-in detectors connected to the photomultiplier output and referenced to either the vibrating plate or chopper wheel measures  $\Delta I$  or  $I(\lambda_o)$ , respectively, and by taking the ratio, we obtain

$$\frac{\Delta I}{I} = -t \frac{d\alpha}{d\lambda} \Delta\lambda, \quad (2)$$

using the Beer-Lambert law

$$I = (1 - R)^2 I_0 e^{-\alpha t}. \quad (3)$$

Here,  $I_0$  is the light intensity incident on the sample and  $t$ ,  $R$ , and  $\alpha$  are the sample's thickness, reflectivity, and absorption coefficient, respectively. In Eq. (3), we have ignored multiple internal reflections and the wavelength dependence of the incident light and reflectivity, which are known to be negligible in the wavelength region of interest for a suitable choice of sample thickness. We have also neglected the appearance of higher order wavelength derivatives of  $\alpha$ , as we mitigate the size of these terms by fixing the wavelength modulation amplitude equal to the spectral resolution of the monochromator [51].

During the measurement, samples are suspended inside a liquid helium immersion-type dewar with a pumping port for lowering the helium vapor pressure to below the lambda point. In all measurements reported here, the pressure was kept at a constant 2.0 Torr, corresponding to a helium bath temperature of 1.4 K [52]. Optical access to the sample was provided by inner and outer quartz windows on the dewar, which were oriented parallel to the flat faces of the inner Pyrex helium reservoir. Depending on its shape, the sample was mounted to one of several custom-designed aluminum sample holders using low-temperature glue or light contact with nylon screws to minimize strain.

The samples were produced either from boule material or homoepitaxial wafers of 4H-SiC from Cree, Inc. Samples of boule material were sectioned from two 4 cm diameter boules from independent growth runs into rectangular slabs, while free-standing samples of epitaxial material were made by mechanically polishing off the substrate of  $\sim 1$  cm<sup>2</sup> sections from several different (0001) oriented homoepitaxial wafers (with up to a 4° miscut). Substrate removal was carried out using a Strasbaugh polishing wheel and a diamond grit slurry, with the final optical finish being obtained using 0.25- $\mu$ m diamond grit. The reverse side (Si face) was left as-grown. Boule samples were cut such that their cross-sections lay in the (11 $\bar{2}$ 0) planes and mechanically polished in the same manner. The choice to section samples along the (11 $\bar{2}$ 0) plane was made so that light incident on these faces could be polarized either parallel or perpendicular to the  $c$  axis ( $\hat{c}$ ). (0001) oriented free-standing epitaxial layers could therefore only be used to measure the WMA spectrum for light polarized perpendicular to the  $\hat{c}$  axis. To confirm the crystallographic orientation of the boules, transmission Laue images were obtained from a sacrificial slice from each boule before sectioning. Several samples with thicknesses ranging between 50  $\mu$ m and 4 cm were produced so that the WMA spectrum could be measured with high sensitivity for both large and small values of the absorption coefficient. The spectrum was measured in several narrow, overlapping wavelength intervals for which a sample was chosen whose thickness maximized  $\Delta I$ , which from Eqs. (1) and (3) occurs for  $t = \alpha^{-1}$  (the optical penetration depth). Room-temperature measurements of the penetration depth have already been obtained over a wide wavelength range [53], and have been used as a rough guide for this purpose.

The purity of the samples was verified from the calibrated ratio of the Q<sub>o</sub> nitrogen-bound exciton recombination line to the I<sub>77</sub> free exciton recombination line in LTPL [54,55], which showed nitrogen concentrations in the low 10<sup>15</sup> cm<sup>-3</sup> to 10<sup>13</sup> cm<sup>-3</sup> range for the boule and epitaxial material, respectively. In order to measure the LTPL, samples were suspended in a pumped liquid helium immersion dewar of similar design to the one described above and illuminated with an optically pumped semiconductor laser (Genesis CX-355) with wavelength  $\lambda_{ex} = 3550$  Å. In order to measure the LTPL polarized either parallel or perpendicular to the  $c$ -axis, free-standing epitaxial layers were oriented with the beam at normal incidence to their cross-section, while the photoluminescence was collected from their edge, as in the arrangement shown in Fig. 3(b) of Ref. [24]. Boule samples were oriented with their (11 $\bar{2}$ 0) cross-section facing the photoluminescence

collection path, with the laser beam incident on the same face at a glancing angle. The collected photoluminescence would then be collimated, polarized with a Glan-Thompson prism, and focused onto the entrance slit of an asymmetric, Fast-Fastie type spectrometer equipped with a liquid nitrogen cooled CCD.

For all samples, the laser was focused with a <1 mm diameter spot size, and the incident power was kept at the minimum level required ( $\sim 1$  mW) to obtain a reasonable signal-to-noise ratio. This was done in order to reduce sample heating and thermally-induced broadening of the lines observed in the LTPL. For the helium pumping system used to measure LTPL, we could obtain a bath temperature as low as 2 K, which was again determined from the helium vapor pressure. The linewidths of the free exciton recombination radiation indicated that the free exciton ensemble was in good thermal equilibrium with the bath before recombination, and the exciting illumination induced minimal sample heating.

For the WMA spectra we present below in Secs. IV through X, the samples used were generally boule samples, as they could be cut and polished to a wide range of desired thicknesses and the incident light could be polarized both parallel and perpendicular to their  $c$ -axis. As described in the next section, free-standing epitaxial layers were generally used to measure LTPL as these were of a higher purity than the boule samples and so produced very little nitrogen-bound exciton photoluminescence that might otherwise obscure the free exciton photoluminescence of interest. Although not shown here, LTPL was measured on samples from the boule material and WMA spectra were measured on free-standing epitaxial layers (for light polarized perpendicular to  $\hat{c}$  only) to check for consistency in the locations of spectral features relating to free exciton absorption or recombination. Our findings indicate that, for the boule and epitaxial samples studied here, the spectral features described in the following results sections are common to both groups of samples, and so we do not attempt to give a detailed comparison between the LTPL and WMA spectra of boule and epitaxial 4H-SiC.

### III. THEORY

For indirect semiconductors, the fundamental absorption edge is characterized by a series of abrupt onsets of absorption, each of which is associated with the threshold photon energy  $\hbar\omega_a = E(\vec{k}_c) + \hbar\Omega$  required to create a momentum-conserving phonon with energy  $\hbar\Omega$  (phonon absorption is negligible at our experimental temperatures) and a free exciton in its ground state  $E(\vec{k}_c)$ . It is assumed here that the exciton is made up of an electron localized at the wave vector  $\vec{k}_e = \vec{k}_c$  of the lowest conduction band minimum (in this case, the  $M$  point) and a hole localized at the wave vector  $\vec{k}_h = 0$  of the highest valence band maximum. Beyond this threshold, excitons are produced with wave vector  $\vec{K} \neq \vec{k}_c$  and energy  $E(\vec{K}) > E(\vec{k}_c)$  ( $\vec{K}$  is the wave vector associated with the exciton center of mass). Elliott has shown that in a semiconductor with spherical, parabolic valence and conduction bands, the absorption coefficient due to the creation of free, indirect excitons may be expressed as [56]

$$\alpha \sim (\hbar\omega - E(\vec{k}_c) - \hbar\Omega)^{1/2}. \quad (4)$$



In this hydrogenic model for the exciton, its energy dispersion  $E(\vec{K})$  is also spherical and parabolic about the point  $\vec{K} = \vec{k}_c$ . The square-root dependence of the absorption coefficient is a consequence of the parabolic dependence of  $E$  on  $\vec{K}$ , which in turn is a consequence of the parabolic dispersion of the model valence and conduction band extrema (in Sec. IX, we will see how this assumption breaks down for the case of 4H-SiC when  $\vec{K}$  moves away from the position of the minimum). The wavelength derivative of the absorption coefficient in the vicinity of such a threshold is then given by

$$\frac{d\alpha}{d\lambda} \sim -(\hbar\omega)^2(\hbar\omega - E(\vec{k}_c) - \hbar\Omega)^{-1/2}. \quad (5)$$

We include the effect of finite exciton lifetime by making the substitution  $E(\vec{K}) \rightarrow E(\vec{K}) + i\eta$  (where  $\eta$  is a lifetime broadening parameter), which transforms this dependence into the following form [48,49]:

$$\frac{d\alpha}{d\lambda} \sim -\frac{\sqrt{\sqrt{x^2 + 1} + x}}{\sqrt{x^2 + 1}}, \quad (6)$$

where  $x = (\hbar\omega - \hbar\omega_a)/\eta$  [we ignore the slowly varying  $(\hbar\omega)^2$  factor in Eq. (5)]. Note that, in addition to broadening the inverse-square-root-type peaks in the WMA spectrum, the lifetime broadening parameterized by  $\eta$  also shifts the peak position from the actual absorption threshold energy  $\hbar\omega_a$  up by an amount  $\eta/\sqrt{3}$ . For some of the absorption onsets to be discussed below (namely: those in Secs. VI and VII),  $\eta$  may be as large as a few meV, and so fitting the data to Eq. (6) rather than simply measuring peak positions becomes especially important for obtaining accurate measurements of  $\hbar\omega_a$ .

Using the energies of the momentum-conserving phonons, it follows that a precise determination of the threshold energies  $\hbar\omega_a$  can be used to obtain the ground state energy  $E(\vec{k}_c)$  of the exciton, which, for the exciton whose electron lies in the lowest conduction band minimum and whose hole lies in the topmost valence band maximum, is related to the fundamental band gap  $E_g$ :

$$E(\vec{k}_c) = E_{gx} = E_g - E_x, \quad (7)$$

where  $E_{gx}$  is the exciton band gap and  $E_x$  is the binding energy of the exciton. In the remaining discussion, we will refer to this exciton as EX<sub>fg</sub>, where the subscript “fg” emphasizes that the exciton is associated with the fundamental gap (namely, the electron occupies the lowest conduction band minimum and the hole occupies the topmost valence band maximum). Likewise, we will refer to the exciton whose hole instead occupies the spin-orbit split-off or crystal-field split-off valence band maximum by EX<sub>so</sub> or EX<sub>cf</sub>, respectively. The exciton whose hole occupies the uppermost valence band maximum and whose electron occupies the second lowest conduction band minimum we will refer to by EX<sub>c2</sub>. To all three of these latter classes of excitons will be associated a unique binding energy ( $E_{x,so}$ ,  $E_{x,cf}$ , and  $E_{x,c2}$ , respectively) and  $E$  versus  $\vec{K}$  dispersion, whose minimum energy may be expressed in a form identical to that shown in Eq. (7) but with  $E_g$  replaced by the energy gap appropriate to the occupied band extrema and the binding energy replaced with that which is particular to the exciton in question.

Within the hydrogenic model for the exciton, the energy dispersion for each one of these excitons in fact consists of a hydrogenic series of bands  $E_n(\vec{K})$ , each one parabolic, spherical, and with their minima all located at the same point in the Brillouin zone. For each exciton, we will refer to the lowest of these minima as the ground state of that exciton. While Eq. (7) represents the energy of the lowest of these minima (i.e., that for  $n = 1$  state of the EX<sub>fg</sub> exciton), the energies of the remaining minima are given by [56]

$$E_n(\vec{k}_c) = E_g - E_x/n^2. \quad (8)$$

The relative energy separations of these minima are then proportional to the exciton binding energy. This may be calculated analytically in the hydrogenic model [56]:

$$E_x = \frac{\mu e^4}{2\hbar^2 \epsilon^2}, \quad (9)$$

where  $\mu$  is the reduced mass of the electron-hole pair and  $\epsilon$  is the static dielectric constant. Even though this model is probably a poor approximation for the case of 4H-SiC, we estimate  $E_x$  by first taking a suitable average over the tensoral components of the electron and hole effective mass tensors to compute  $\mu$ :

$$\frac{1}{\mu} = \frac{1}{m_{e,avg}} + \frac{1}{m_{h,avg}}, \quad (10)$$

$$\frac{1}{m_{e,avg}} = \frac{1}{3} \left( \frac{1}{m_{e,ML}} + \frac{1}{m_{e,MK}} + \frac{1}{m_{e,M\Gamma}} \right), \quad (11)$$

$$\frac{1}{m_{h,avg}} = \frac{1}{3} \left( \frac{1}{m_{h,\parallel}} + \frac{2}{m_{h,\perp}} \right). \quad (12)$$

Using  $m_{e,ML} = 0.33m_0$ ,  $m_{e,MK} = 0.31m_0$ ,  $m_{e,M\Gamma} = 0.58m_0$  [57],  $m_{h,\parallel} = 1.75m_0$ ,  $m_{h,\perp} = 0.66m_0$  [58], and  $\epsilon \approx 10$  [59], we find  $E_x = 40$  meV and an energy separation  $3E_x/4 = 30$  meV between the  $n = 1$  and  $n = 2$  states for the fundamental gap exciton EX<sub>fg</sub>. While  $n > 1$  indirect excitons have been observed in the absorption spectra of other materials [44,60], we have not observed any splittings of this magnitude in the WMA spectrum of 4H-SiC to suggest that such excited states have been observed. Furthermore, it is expected that exciton states with  $n > 1$  would be more difficult to detect, since the associated transition rates scale as  $n^{-3}$  in the hydrogenic model [56]. We will therefore confine the remaining discussion to the  $n = 1$  ground state of the excitons EX<sub>fg</sub>, EX<sub>so</sub>, EX<sub>cf</sub>, and EX<sub>c2</sub>. Later, in Sec. X, we will discuss the degeneracies of the exciton ground state, and how they may be broken by both spatial and spin degrees of freedom of the electron and hole.

Because, as mentioned above in Sec. I, the valence and conduction band extrema associated with these excitons are all at or very near to the  $\Gamma$  or  $M$  points, respectively, the same phonons will participate in the corresponding indirect transitions in all cases: namely, the principal phonons with wave vector also lying at the  $M$  point. In 4H-SiC there are 24 principal phonons, each of which is nondegenerate. Most of their energies have been determined from LTPL measurements, for which the phonons participate in the indirect recombination of both free and impurity-bound excitons. Historically, the quality of the material used in these measurements was such that the phonon energies were determined

from the LTPL of nitrogen-bound excitons, which produced the greatest integrated intensity near the band edge [24,61,62]. In 4H-SiC, the LTPL from nitrogen-bound excitons consists of two no-phonon lines,  $P_o$  and  $Q_o$  (which correspond to the two inequivalent C sites in the unit cell), and their phonon replicas at longer wavelengths. These are intermingled with the (usually weaker) lines due to recombination of free excitons, which from energy and momentum conservation appear at  $\hbar\omega_e = E_{gx} - \hbar\Omega$  (again, we assume phonon absorption is not observed at low temperature). The relative spacings of the nitrogen-bound exciton's phonon replicas closely resemble those of the free exciton lines, and so it has been assumed that the offsets of the phonon replicas from their corresponding no-phonon lines are equal to the energies of the same momentum-conserving phonons which participate in the recombination of free excitons.

However, in contrast to free exciton recombination, it is not immediately obvious how energy and momentum conservation should apply in the case of a bound exciton, whose wave function is not localized to one point of the Brillouin zone. This issue has been addressed in the case of the nitrogen-bound exciton in GaP, where the extent to which the exciton was localized produced up to a 2 meV shift in the calculated offset of the TA phonon replica from its no-phonon line [63]. Since nitrogen behaves as an isoelectronic trap in GaP [64] and a shallow donor in 4H-SiC [65], it is expected that the degree to which the exciton is localized (and, by extension, the shift in the observed phonon energies) will be smaller in the latter case. Nevertheless, to avoid this potential source of error, we have measured the LTPL of an ultrahigh-purity (nitrogen concentration  $n \sim 10^{13} \text{ cm}^{-3}$ ) free-standing 4H-SiC epitaxial layer, which produces substantially stronger free exciton photoluminescence than bound exciton photoluminescence, and allows for a straightforward determination of the principal phonon energies. The free exciton recombination lines have a form with a square-root-type dependence that is similar to that of the abrupt onsets in the absorption coefficient, but includes an additional Boltzmann factor which reflects their thermal distribution immediately prior to recombination [66]:

$$I \sim \sqrt{\hbar\omega - \hbar\omega_e} e^{-(\hbar\omega - \hbar\omega_e)/k_B T}, \quad (13)$$

where  $k_B$  is Boltzmann's constant and it is presumed  $\hbar\omega > \hbar\omega_e$ . For a given phonon, we obtain the pair  $\hbar\omega_a$  and  $\hbar\omega_e$  from fits of the form Eqs. (6) and (13) to the WMA and LTPL spectra, respectively, which in turn may be used to compute the exciton band gap and the phonon energy:

$$E_{gx} = (\hbar\omega_a + \hbar\omega_e)/2, \quad (14)$$

$$\hbar\Omega = (\hbar\omega_a - \hbar\omega_e)/2. \quad (15)$$

The above method assumes one has identified absorption onsets  $\hbar\omega_a$  and LTPL lines  $\hbar\omega_e$  associated with the same exciton, namely,  $EX_{fg}$ . We ensure this from the fact that, at  $T = 2 \text{ K}$ , LTPL from the higher energy excitons,  $EX_{so}$ ,  $EX_{cf}$ , and  $EX_{c2}$  is not present, and by exploiting the fact that the  $\hbar\omega_a$  appear at energies symmetric to  $\hbar\omega_e$  about the exciton band gap  $E_{gx}$ . In this way, we can also readily identify those features in

the WMA spectrum which are due to excitons other than the fundamental gap exciton  $EX_{fg}$ .

#### IV. OVERVIEW OF NEAR-EDGE ABSORPTION

In Fig. 3, we show an overview of our WMA measurements within the first  $\sim 100 \text{ meV}$  of the fundamental absorption edge for light polarized with its electric field  $\vec{E} \parallel \hat{c}$  and  $\vec{E} \perp \hat{c}$ . The spectra consist of a dense series of sharp, asymmetric peaks that exhibit the characteristic inverse-square-root shape given in Eq. (5) that indicates free indirect exciton absorption. In Table I, we give a summary of the phonon energies determined from our combined WMA and LTPL spectra and compare them with calculated values [18] and values measured previously from nitrogen bound exciton LTPL [24,61]. We equate phonons listed on the same row in the table, although we note that none of the three experimental data sets listed here accounts for all 24 principal phonon modes (phonon dispersion calculations [18–24] suggest that several  $M$  point phonons might be unresolved in the LTPL measured so far).

For the most part, the observed discrepancies fall within our  $\pm 0.6 \text{ meV}$  experimental error in the *absolute energies* of the phonons, although the discrepancies in some small relative energy separations likely cannot be accounted for by experimental error. For instance, we obtain a  $0.6 \pm 0.1 \text{ meV}$  energy difference between the 40.6 and 41.2 meV phonons, whereas for references [24] and [61] the energy difference is 1.3 and 1.1 meV, respectively.

This discrepancy can be directly seen in Fig. 4, which shows a segment of our own LTPL measurements in which appear the 40.6 and 41.2 meV phonon-assisted free exciton lines alongside the nitrogen-bound exciton lines  $P_{40,3}$  and  $P_{41,4}$  (the subscripts denote their energy offset in meV from  $P_o$ ). The smaller energy separation for the former two is apparent not only from the fits to the data but also from the lesser extent to which they are resolved compared to that of the latter two. A theoretical study of the nitrogen-bound exciton in SiC similar to the one mentioned earlier for GaP [63] may help to answer whether it is the localization of the bound exciton which is responsible for these apparent deviations, but for the present purposes we simply take this as justification for our independent determination of the principal phonon energies.

#### V. SPIN-ORBIT SPLITTING OF THE VALENCE BAND MAXIMUM

In contrast to the LTPL spectrum at 2 K, each principal phonon gives rise to two peaks in the WMA spectrum shown in Fig. 3, which is due to the spin-orbit splitting of the valence band maximum. The lower energy peak in a given pair corresponds to creation of exciton  $EX_{fg}$  while the higher energy peak corresponds to the creation of exciton  $EX_{so}$ . The energy separation between the two peaks in a given pair is equal to the spin-orbit splitting  $\Delta_{so}$  of the valence band maximum up to the difference in binding energies for the two excitons:

$$\hbar\omega_{so} - \hbar\omega_{fg} = \Delta_{so} + E_x - E_{x,so} \equiv \Delta'_{so}. \quad (16)$$

We list the measured spin-orbit splittings for each individual phonon in Table I, and from the average, we find  $\Delta'_{so} = 7.0 \pm 0.6 \text{ meV}$ , which agrees well with the  $6.8 \pm 0.6 \text{ meV}$  obtained

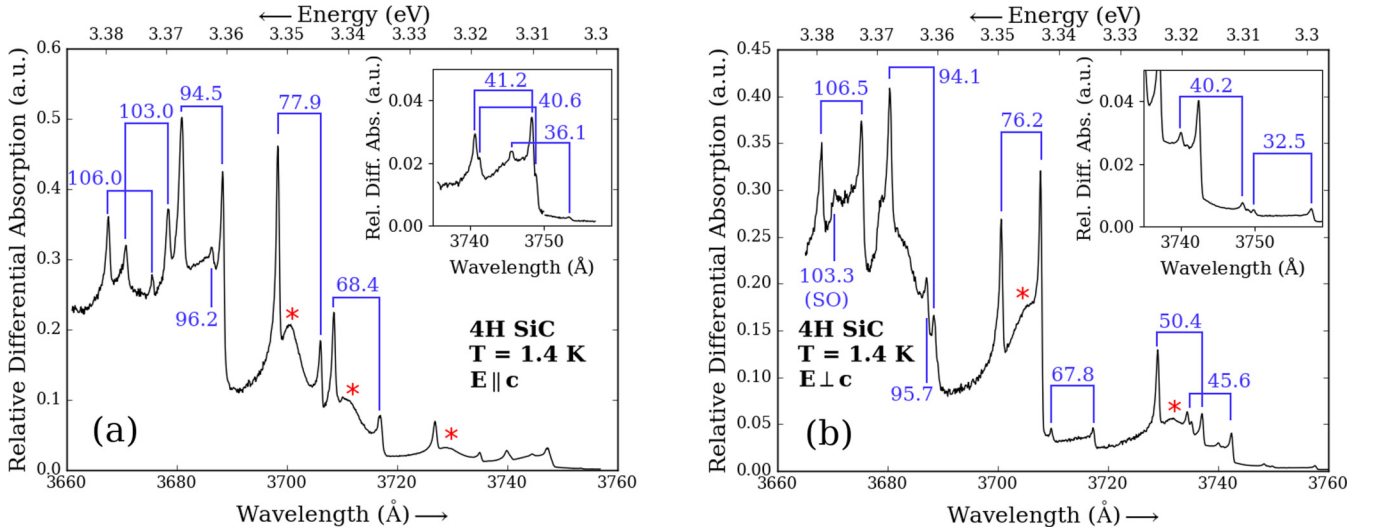


FIG. 3. Overview of wavelength-modulated absorption measurements within the first  $\sim 100$  meV of the fundamental absorption edge in  $4H$ -SiC at 1.4 K. The incident light is polarized with its electric field (a)  $\vec{E} \parallel \hat{c}$  or (b)  $\vec{E} \perp \hat{c}$ . The spin-orbit splitting of the valence band results in pairs of peaks throughout the absorption edge which are labeled by brackets and the energy in meV of the momentum-conserving phonon participating in the indirect transition from the two topmost valence band maxima to the lowest conduction band minimum. Asterisks indicate features due to nonparabolicity in the valence bands, described in Sec. IX. Insets show expanded views of the absorption onsets due to the lowest energy principal phonons.

from previous WMA measurements of  $4H$ -SiC [30] (note that we do not measure  $\Delta'_{so}$  for the 96.2, 95.7, and 103.3 meV phonons, for which one of the two spin-orbit split peaks overlaps with a peak due to another phonon). We also find fair agreement with the values  $\Delta_{so} = 8.6$  and  $8.2$  meV obtained

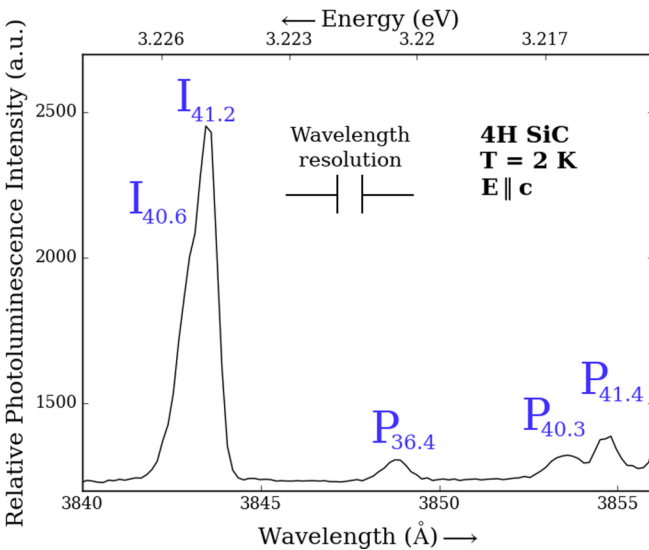


FIG. 4. Expanded view of several peaks in the low-temperature photoluminescence spectrum of  $4H$ -SiC. Peaks labeled  $I_{\hbar\Omega}$  are due to recombination of free excitons with emission of a phonon with energy  $\hbar\Omega$ , and peaks labeled  $P_{\hbar\Omega}$  are due to recombination of nitrogen-bound excitons with emission of a phonon with energy  $\hbar\Omega$  (all energies expressed in meV). The phonon energies associated with the free exciton are determined as described in the text, whereas those associated with the bound exciton are determined from the corresponding line's separation from the  $P_0$  no-phonon line (not shown).

from the relativistic band structure calculations of Persson and Lindelfelt [16] and Lyu and Lambrecht [34], respectively, which suggests from Eq. (16) that the binding energy for the fundamental gap exciton  $EX_{fg}$  is slightly less than that of the spin-orbit split-off exciton  $EX_{so}$ . The fact that the two binding energies appear to be comparable would be expected if the two valence band maxima had similar hole effective masses, which appears to be true from band structure calculations [16].

Alongside the phonon energies of Table I, we have also given the corresponding calculated phonon symmetries [20,34]. These are labeled according to the single group representations of the  $C_{2v}$  point group, which are associated with the  $M$  point of the Brillouin zone (note that we use the Koster *et al.* notation throughout [67]). The selection rules for indirect transitions between valence band maxima at the  $\Gamma$  point and conduction band minima at the  $M$  point are determined in part by these phonon symmetries, as has been described by Sridhara *et al.* [30]. Taking the valence band maximum to have  $\Gamma_5$  symmetry and the lowest conduction band minimum to have  $M_4$  symmetry (as determined from band structure calculations [16,18]), their group theory analysis of the selection rules shows that  $M_1$  and  $M_3$  symmetry phonons participate in indirect transitions for light polarized  $\vec{E} \parallel \hat{c}$  and  $M_2$  and  $M_4$  symmetry phonons participate for light polarized  $\vec{E} \perp \hat{c}$ .

We note that the selection rules from which this result follows have been derived while ignoring electron spin. With spin included, the twofold degeneracy of the  $\Gamma_5$  valence band maximum is broken into two doubly degenerate valence band maxima:

$$\Gamma_5 \otimes \Gamma_7 = \Gamma_7 \oplus \Gamma_9, \quad (17)$$

where electron spin is represented by the  $\Gamma_7$  double group representation of  $C_{6v}$  (we ignore small relativistic terms which displace the maxima from the  $\Gamma$  point). Neglecting electron

TABLE I. Comparison between principal phonon energies as measured in this work from free exciton wavelength-modulated absorption (WMA) and low-temperature photoluminescence (LTPL) (for  $\vec{E} \parallel \hat{c}$  or  $\vec{E} \perp \hat{c}$ ), those measured in the works of Choyke *et al.* [61] and Ivanov *et al.* [24] from nitrogen bound exciton LTPL, and those calculated in the work of Lyu and Lambrecht [18] and Serrano *et al.* [20]. In Refs. [18,20,24], the authors have identified their phonon energies with those of Refs. [24,61], and the listing of the phonon energies in columns two through four reflect those identifications. The phonon energies of this work were measured from both WMA and LTPL using Eq. (15) with the exception of the 103.3 meV phonon, which was obscured in the WMA spectrum by an overlapping spin-orbit split-off absorption onset due to another phonon. This phonon energy was measured in LTPL only, assuming an exciton band gap  $E_{gx}$  of 3.2659 eV [average  $E_{gx}$  determined from Eq. (7) for the other phonons]. The remaining four columns show, for each phonon measured in this work the measured spin-orbit splitting  $\Delta'_{so}$ , the ratio of the associated peak amplitudes  $A_{so}$  and  $A_{fg}$  in the WMA spectrum for the spin-orbit split-off and fundamental gap free exciton, respectively [as determined from fits to the function given by Eq. (6)], and the phonon symmetry as calculated in Ref. [34] or [20]. Note that the symmetry labels of Ref. [34] are corrections of those given in Ref. [18] in which  $M_2$  symmetry labels are interchanged with  $M_4$  symmetry labels. Respective energy uncertainties in columns five and six are approximately  $\pm 0.6$  and  $\pm 0.2$  meV. Dashes in columns six and seven indicate where a spin-orbit splitting was not observed (due to overlap with other features in the WMA spectrum), and the remaining dashes indicate phonons that were not observed or were not matched with those calculated in Ref. [18].

	Ref. [61]: $\hbar\Omega$ (meV)	Ref. [24]: $\hbar\Omega$ (meV)	Ref. [18]: $\hbar\Omega$ (meV)	Ref. [20]: $\hbar\Omega$ (meV)	This work: $\hbar\Omega$ (meV)	This work: $\Delta'_{so}$	This work: $A_{so}/A_{fg}$	Ref. [34]: Phonon symmetry <sup>c</sup>	Ref. [20]: Phonon symmetry <sup>c</sup>
$\vec{E} \parallel \hat{c}$									
	36.5	36.6	35.9	34.9	36.1	7.4	$4 \pm 1$	$M_1$	$M_1$
	40.6	40.6	40.5	38.7	40.6	6.6	$0.88 \pm 0.07$	$M_3$	$M_3$
	41.7	41.9	40.9	39.4	41.2	6.6	$0.60 \pm 0.02$	$M_3$	$M_3$
	52.7	52.7	51.9	51.3	52.3	7.2	$3.5 \pm 0.4$	$M_1$	$M_1$
	68.7	68.8	68.2	68.5	68.4	7.4	$2.5 \pm 0.2$	$M_1$	$M_1$
	78.5	78.0	75.8	75.8	77.9	7.2	$2.85 \pm 0.06$	$M_1$	$M_1$
	-	-	94.5 <sup>a</sup>	-	-	-	-	$M_3$	-
	96.1	94.7	94.8	93.2	94.5	6.7	$0.64 \pm 0.02$	$M_3$	$M_3$
	-	-	95.5 <sup>a</sup>	-	-	-	-	$M_1$	-
	97.8	96.5	96.7	94.4	96.2	-	-	$M_1$	$M_3$
	101.6	-	-	94.9	-	-	-	-	$M_1$
	105.6	103.5	103.6	96.9	103.0	7.0	$0.8 \pm 0.2$	$M_1$	$M_1$
	108.2	106.3	106.6	103.5	106.0	7.4	$4 \pm 1$	$M_1$	$M_1$
	-	109.5	-	-	-	-	-	-	-
$\vec{E} \perp \hat{c}$									
	33.0	33.2	32.5	32.5	32.5	6.8	$0.44 \pm 0.06$	$M_2$	$M_2$
	41.0	41.1	40.3	39.4	40.2	7.3	$1 \pm 1$	$M_4$	$M_4$
	46.1	46.3	45.4	45.1	45.6	6.6	$0.41 \pm 0.01$	$M_2$	$M_2$
	50.8	50.9	50.1	50.2	50.4	7.2	$2.06 \pm 0.06$	$M_4$	$M_4$
	67.8	68.1	67.6	67.8	67.8	6.8	$0.8 \pm 0.2$	$M_4$	$M_4$
	76.6	76.3	77.5	74.7	76.2	6.6	$0.50 \pm 0.02$	$M_4$	$M_4$
	-	94.5	94.3	93.0	94.1	7.3	$10 \pm 1$	$M_2$	$M_2$
	-	94.5	94.8 <sup>b</sup>	-	-	-	-	$M_2$	-
	97.3	96	95.9	94.0	95.7	-	-	$M_4$	$M_4$
	99.1	-	-	94.4	-	-	-	-	$M_2$
	100.3	98.9	98.8	97.5	-	-	-	$M_4$	$M_4$
	106.3	103.9	104.2	102.5	103.3	-	-	$M_4$	$M_4$
	108.7	106.8	106.8	-	106.5	6.7	$0.7 \pm 0.2$	$M_4$	-

<sup>a</sup>Tentatively assigned in [18] to 94.7 meV phonon in [24].

<sup>b</sup>Tentatively assigned in [18] to 94.5 meV phonon in [24].

<sup>c</sup>The notation for symmetry labels is that of Koster *et al.* [67]. In Ref. [34], the chosen coordinate system is such that the roles of the  $x$  and  $y$  basis functions are interchanged relative to those of Koster *et al.* The coordinate system chosen in Ref. [20] was not given.

spin in the selection rules just described therefore accounts only for the symmetries of the spatial components of the wave functions for the top two valence bands. In a way, this is analogous to the LS coupling limit commonly applied to the optical transitions of atoms, in which the atomic wave functions are considered as a simple direct product of spatial and spin wave functions and the selection rules are determined for the spatial and spin parts separately. Later, in Sec. X, we shall examine the consequences of introducing spin into the group theory

analysis of the selection rules, but for the present purposes we shall assume they apply equally to the top two valence band maxima, by virtue of their having both been derived from  $\Gamma_5$  symmetry spatial wave functions.

For each phonon, we have also measured the relative amplitudes  $A_{fg}$  and  $A_{so}$  of the peaks in the WMA spectrum corresponding to  $EX_{fg}$  and  $EX_{so}$ , respectively (the amplitudes  $A_{fg}$  and  $A_{so}$  are the multiplicative scaling factors of the function in Eq. (6) used to fit to the individual peaks in the



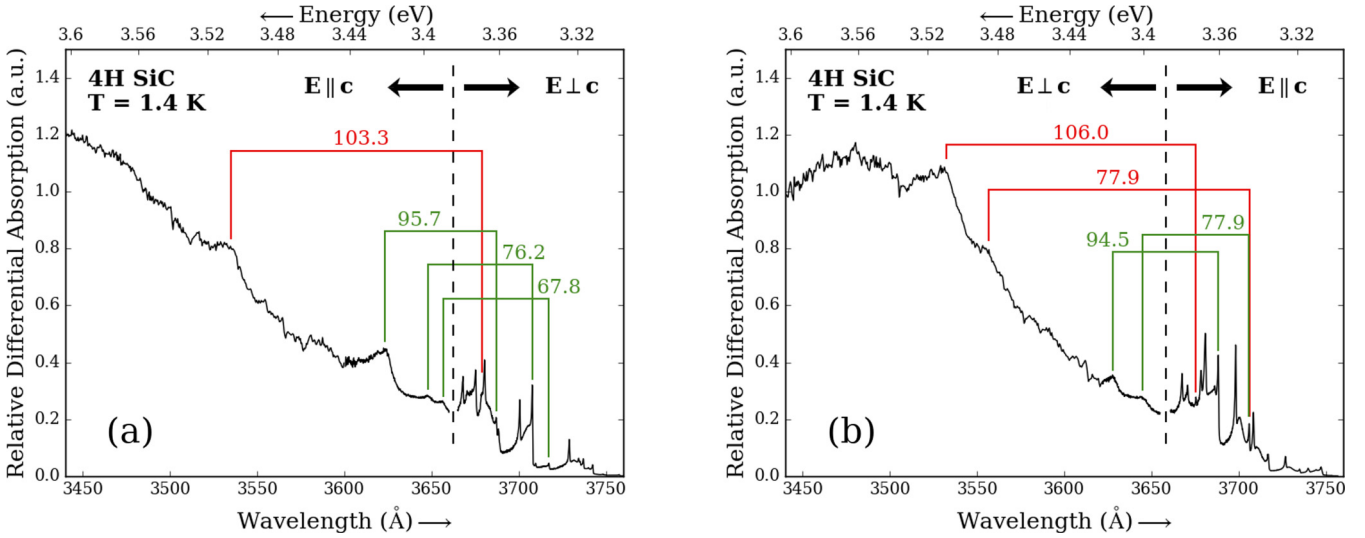


FIG. 5. Wavelength-modulated absorption spectrum of 4H-SiC measured over the full wavelength range described in this report. For wavelengths shorter than  $\sim 3660$  Å, we observe several broad features due to indirect transitions either from the third highest (crystal-field split-off) valence band maximum to the lowest conduction band minimum or from the topmost valence band maximum to the second lowest conduction band minimum. Selection rules indicate that each of these features is split-off from a lower energy, indirect transition between the topmost valence band maximum and lowest conduction band minimum and which involves the same phonon but *opposite* polarization. The splittings due to the crystal-field splitting are shown with green brackets, and the splittings due to the second lowest conduction band are shown with red brackets. The energy in meV of the participating phonon is shown alongside the brackets, and the polarization of the spectrum shown is interchanged between  $\vec{E} \parallel \hat{c}$  and  $\vec{E} \perp \hat{c}$  to show both peaks in a given pairing in the same plot.

WMA spectrum). Interestingly, from Table I we may observe that, for  $\vec{E} \parallel \hat{c}$ ,  $A_{fg} < A_{so}$  for phonons with symmetry  $M_1$  (with the exception of the 103.0 meV phonon), and  $A_{fg} > A_{so}$  for phonons with symmetry  $M_3$ . This might be expected on the basis that the phonon symmetry is contained implicitly in the electron-phonon interaction  $H_\Omega$  through the atomic displacements  $\delta\vec{R}_{l,a}$  about their equilibrium positions  $\vec{R}_{l,a}$  [68]

$$H_\Omega = \sum_{l,a} \delta\vec{R}_{l,a} \cdot \vec{\nabla}_{\vec{r}} V_a(\vec{r} - \vec{R}_{l,a}). \quad (18)$$

In the above,  $l$  and  $a$  index the crystal's unit cells and the atomic positions within each unit cell, respectively, and  $V_a(\vec{r} - \vec{R}_{l,a})$  is the electrostatic potential energy due to the atom located at  $\vec{R}_{l,a}$  as seen by an electron at position  $\vec{r}$ . While the atomic displacement field  $\delta\vec{R}_{l,a}$  should be different for each of the 24 principal phonon modes, the results outlined in Table I seem to suggest that the electron-phonon interaction is determined to a large extent by which of the two symmetry representation,  $M_1$  or  $M_3$ , they belong to.

The electron-phonon interaction has recently been calculated from first principles and studied in relation to the LTPL spectrum in 4H-SiC by Lyu and Lambrecht [18], however their work did not include the spin-orbit interaction or exciton effects. To our knowledge there are no theoretical studies which include these effects in treating indirect transitions in 4H-SiC, nor has there been any experimental work to measure the strength of the electron-phonon and electron-hole interactions for the principal phonon modes involved in fundamental absorption edge transitions (as may be determined from absorption measurements with applied uniaxial stress [69–71]). Such studies would be needed in order to bring further insight

into the correlation described above. In any case, it seems to bring qualitative support to the assigned phonon symmetries listed in Table I, at least for those phonons participating in the  $\vec{E} \parallel \hat{c}$  polarization. The comparative lack of correlation for the  $\vec{E} \perp \hat{c}$  polarization is currently not understood, although it may be related to similar behavior in the correlation between the measured spin-orbit splittings  $\Delta'_{so}$  and the phonon symmetries, which can be explained on the basis of fine structure splittings in the exciton ground state (see Sec. X).

## VI. CRYSTAL-FIELD SPLITTING

In Fig. 5, we show the full range of our WMA measurements in 4H-SiC. The figure includes the wavelength interval shown in Fig. 3, which spans the long wavelength end of the two plots down to about 3660 Å, while at shorter wavelengths we observe a comparatively featureless background which steadily increases with decreasing wavelength. On top of this background appear eight broad, asymmetric peaks, four for  $\vec{E} \parallel \hat{c}$  and four for  $\vec{E} \perp \hat{c}$ , which are roughly grouped into a set of five lying at longer wavelengths and a set of three lying at shorter wavelengths. Despite their considerable breadth, each of these features can be adequately fit to Eq. (6), which is applicable to free, indirect exciton absorption as long as the broadening parameter  $\eta$  is treated as a free parameter. Based on their relative energy spacings, we identify the five lower energy absorption onsets as indirect transitions from the crystal-field split-off valence band maximum at  $\Gamma$  to the lowest conduction band minimum at  $M$ .

Since the crystal-field split-off valence band maximum lies at the same point ( $\Gamma$ ) as the top two valence band maxima, the principal phonons summarized in Table I will also be active in these indirect transitions. In analogy with the spin-orbit

TABLE II. Energies  $\hbar\omega_a$  of the absorption onsets due to the crystal-field split-off valence band maximum, as obtained from fits to Eq. (6), energies  $\hbar\Omega$  of the associated principal phonon, and energy separations  $\Delta'_{cf}$  of  $\hbar\omega_a$  from the corresponding absorption onset due to the fundamental gap exciton  $EX_{fg}$  and the same principal phonon. We estimate the uncertainty in  $\hbar\omega_a$  and  $\Delta'_{cf}$  to be  $\pm 3$  meV.

	$\hbar\omega_a$ (eV)	$\hbar\Omega$ (meV)	$\Delta'_{cf}$ (meV)
$\vec{E} \parallel \hat{c}$	3.389	67.8	55
	3.397	76.2	55
	3.420	95.7	58
$\vec{E} \perp \hat{c}$	3.399	77.9	55
	3.416	94.5	56

splittings  $\Delta'_{so}$  defined in Eq. (16), we therefore expect those onsets due to the crystal-field split-off exciton  $EX_{cf}$  to be split off towards higher photon energies from those of the fundamental gap exciton  $EX_{fg}$  by an amount

$$\Delta'_{cf} \equiv \Delta_{cf} + E_x - E_{x,cf}, \quad (19)$$

where  $E_x$  and  $E_{x,cf}$  are the binding energies for the fundamental gap exciton  $EX_{fg}$  and crystal-field split-off exciton  $EX_{cf}$ , respectively.

In this case, however, the spatial component of the hole wave function should have  $\Gamma_1$  rather than  $\Gamma_5$  symmetry [16,18], and so the selection rules will in general be different. The group theory analysis of the selection rules has already been carried out by Sridhara *et al.* for the case without spin [30]. In summary, if we again take the conduction band to have  $M_4$  (spatial) symmetry [16,18], we find that  $M_1$  and  $M_3$  symmetry phonons participate for  $\vec{E} \perp \hat{c}$  and only  $M_4$  symmetry phonons participate for  $\vec{E} \parallel \hat{c}$ . In other words, for phonons with symmetry other than  $M_2$ , the polarization for which they are active is opposite what it is for transitions associated with excitons  $EX_{fg}$  and  $EX_{so}$ , while  $M_2$  symmetry phonons are not active in either polarization. Each absorption onset associated with  $EX_{cf}$  must therefore be split-off by an amount  $\Delta'_{cf}$  from an absorption onset appearing in the *opposite polarization* which is due to  $EX_{fg}$  and the same principal phonon. We identify these pairs in Fig. 5 using green brackets while also interchanging the polarization at about 3660 Å so that both peaks in a given crystal-field split pair could be shown in the same plot.

In Table II, we give the energies  $\hbar\omega_a$  of the absorption onsets due to the crystal-field split-off valence band maximum as well as their assigned principal phonons and associated crystal-field splittings  $\Delta'_{cf}$ . From this result we obtain an average value  $\Delta'_{cf} = 56 \pm 3$  meV, which falls on the low end of the somewhat broad range 45–130 meV obtained for  $\Delta_{cf}$  from band structure calculations [11,13–16,34] (recall from Eq. (19) that  $\Delta'_{cf}$  and  $\Delta_{cf}$  are equivalent up to a difference in exciton binding energies).

Our result is also consistent with previous WMA measurements of 4H-SiC by Sridhara *et al.* [30], in which a value  $\Delta'_{cf} = 60$  meV was obtained. However, in the case of that experiment, only three absorption onsets were associ-

ated with the crystal-field splitting, while two of these have been identified as being due to the spin-orbit splitting in our results [Sridhara *et al.* claim to observe crystal-field split-off peaks due to the 50.8 and 40.9 meV principal phonons (their measured phonon energies), but these are assigned to spin-orbit split-off absorption onsets due to the 103.0 and 94.1 meV principal phonons in our work]. It seems likely that these were misidentified in the previous work due to the lower wavelength resolution, which obscured the lower energy counterparts to these two spin-orbit split-off absorption onsets. We also note that, while our assignment of the absorption onset at  $\hbar\omega_a = 3.420$  eV to the 95.7 meV principal phonon seems to agree with the assignment to the same onset in the measurements of Sridhara *et al.*, the discrepancy in the measured  $\Delta'_{cf}$  may be accounted for by the fact that Sridhara *et al.* measured the absorption threshold energies  $\hbar\omega_a$  from the positions of the peaks in the WMA spectrum. As described in Sec. IV, the true absorption threshold energies, which are measured in this work, are offset to lower energy from the peaks, and in this particular case by as much as 2 meV.

There is considerably less agreement between our result for the crystal-field splitting and those obtained from electroabsorption [35] and BHEM measurements of 4H-SiC [37]. In the electroabsorption spectra, two rather broad peaks were associated with the crystal-field split-off valence band maximum with emission of a single TA-symmetry phonon mode (the higher energy peak was assigned to an  $n = 2$  state exciton), and a crystal-field splitting of  $83 \pm 2$  or  $88 \pm 3$  meV was obtained depending on the particular TA phonon mode. We note, however, that both peaks were present in the electroabsorption spectra irrespective of the polarization of the incident light, which disagrees with the selection rules. From the BHEM measurements of 4H-SiC, an even larger crystal-field splitting of 110 meV was obtained [37]. Comparison of the results from both electroabsorption and BHEM to our own is made somewhat difficult by the use in the former two measurement techniques of samples with various junctions (pn-, hetero-, or Schottky-type), whereas the interpretation of our measurements, which use high-purity boule material, is comparatively straightforward.

A more direct comparison may be possible in the free carrier absorption measurements of Grivickas *et al.* [32], who observed two distinct spectral features which they attributed to the crystal field splitting (see their Fig. 6). They unfortunately do not identify the participating momentum-conserving phonons, and therefore cannot estimate  $\Delta_{cf}$ . However, the feature they observe appearing at higher incident photon energy seems to correspond with the absorption onset  $\hbar\omega_a = 3.416$  eV listed in our Table II.

## VII. SECOND LOWEST CONDUCTION BAND

As mentioned in the preceding section, the remaining three features on the short wavelength side of Fig. 5 also exhibit the characteristic shape of a broadened indirect absorption onset, although their positions in the WMA spectra are too high in photon energy to be the result of other indirect transitions from the crystal-field split-off valence band maximum with emission of a single phonon. We instead assign these three features to exciton  $EX_{c2}$ , which is associated with indirect

TABLE III. Energies  $\hbar\omega_a$  of the absorption onsets due to the second lowest conduction band minimum, as obtained from fits to expression Eq. (6), energies  $\hbar\Omega$  of the associated principal phonon, and energy separations  $\Delta'_{c2}$  of  $\hbar\omega_a$  from the corresponding absorption onset due to the fundamental gap exciton  $\text{EX}_{\text{fg}}$  and the same principal phonon. We estimate the uncertainty in  $\hbar\omega_a$  and  $\Delta'_{c2}$  to be  $\pm 3$  meV.

	$\hbar\omega_a$ (eV)	$\hbar\Omega$ (meV)	$\Delta'_{c2}$ (meV)
$\vec{E} \parallel \hat{c}$	3.504	103.3	135
$\vec{E} \perp \hat{c}$	3.482	77.9	138
	3.508	106.0	136

transitions from the topmost valence band maximum to the second lowest conduction band minimum. According to band structure calculations [14,16–18,34,38], this minimum lies at the same point ( $M$ ) as the lowest conduction band minimum. Here, again, we need only consider the same principal phonons which participated in the creation of the excitons already discussed in the preceding sections.

In this case, we have again  $\Gamma_5$  for the hole symmetry, but for the electron we take the symmetry to be  $M_1$  according to band structure calculations [16,18]. The selection rules in this case have been worked out by Sridhara *et al.* [30], with the result being that for  $\vec{E} \parallel \hat{c}$   $M_2$  and  $M_4$  symmetry phonons participate in indirect transitions and for  $\vec{E} \perp \hat{c}$   $M_1$  and  $M_3$  symmetry phonons participate. These are the same selection rules as described for exciton  $\text{EX}_{\text{fg}}$  but with the polarizations interchanged. We should then expect these features to be paired with another lying at longer wavelength and *opposite polarization* which is due to the creation of an  $\text{EX}_{\text{fg}}$  exciton and the same principal phonon. The separation  $\Delta'_{c2}$  between each pair is then the energy separation  $\Delta_{c2}$  between the two conduction band minima plus the difference in exciton binding energies, similar to Eqs. (16) and (19). We summarize our assignments of the principal phonons and the corresponding splitting  $\Delta'_{c2}$  for each of the three features in Table III.

In summary, we find  $\Delta'_{c2} = 136 \pm 3$  meV, which falls within what is again a rather broad range 100–180 meV predicted for  $\Delta_{c2}$  by band structure calculations [14,16–18,34,38]. There is better agreement among the experimental values obtained so far. From two BEEM measurements [37,38] of 4H-SiC,  $\Delta_{c2} = 140$  meV is obtained, although in one BEEM measurement [36], no current threshold was observed corresponding to a second conduction band). There is also good agreement with surface photovoltage spectroscopy [39] and free carrier absorption measurements [33] of 4H-SiC, which obtain  $\Delta_{c2} = 130$  and  $115 \pm 10$  meV, respectively.

We must point out that the assignments summarized in Table III represent a revision of our previous estimate of  $\Delta'_{c2} = 144 \pm 2$  meV [31], which was based on several features in the wavelength range 3560 and 3600 Å of the WMA spectrum which failed to reproduce in the larger set of boule and epi samples used in the present study. We therefore limit our assignments to those features which did reproduce for all samples that were measured in this wavelength range. We note

also that, due to the spectral breadth of these absorption onsets (with  $\eta$  between 2 and 10 meV), our present assignments may be appreciably more accurate than those made in our previous measurements, which identified the absorption threshold energies  $\hbar\omega_a$  by their peak positions.

### VIII. LIFETIME BROADENING

There are two chief reasons for the relatively large uncertainty  $\pm 3$  meV in our values for  $\Delta'_{c1}$  and  $\Delta'_{c2}$ . The first has to do with the fact that the absorption onsets due to  $\text{EX}_{c1}$  lie in a wavelength region of relatively small optical penetration depth  $\alpha^{-1}$ , for which thin ( $< 100$   $\mu\text{m}$ ) samples must be used. In this case, mechanical stability of the measurement apparatus becomes a greater concern, since slight drifts or vibrations of the sample in the incident beam will cause different portions of its cross-section to be illuminated. This will in turn lead to a random fluctuation of the transmitted intensity for thin samples with a relatively large fractional thickness variation over their surface, which reduces the signal-to-noise ratio of the measurement.

The more dominant contribution to our uncertainty in  $\Delta'_{c1}$  and  $\Delta'_{c2}$  comes from the intrinsic spectral width (parameterized by  $\eta$ ) of the crystal-field split-off absorption onsets, which greatly exceeds our instrument resolution ( $\delta\lambda \sim 0.1$  Å). Compared to the (likely instrument-limited) values  $\eta = 0.3$  meV obtained for the absorption onsets due to the two lowest energy excitons,  $\text{EX}_{\text{fg}}$  and  $\text{EX}_{\text{so}}$ , we obtain  $\eta = 1$ – $10$  meV for the two higher energy excitons,  $\text{EX}_{c1}$  and  $\text{EX}_{c2}$ . This is an indication that the excitons produced by these latter transitions are considerably more short-lived. Interestingly, the spectral widths for excitons  $\text{EX}_{c1}$  and  $\text{EX}_{c2}$  were not observed to vary appreciably between samples involved in the present study, which included both lightly  $n$ -doped ( $n \sim 10^{15}$   $\text{cm}^{-3}$ ) and ultrapure ( $n \sim 10^{13}$   $\text{cm}^{-3}$ ), free-standing epitaxial wafers. Furthermore, the widths of the crystal-field split-off absorption onsets appear to be comparable to those observed in previous WMA measurements of 4H-SiC by Sridhara *et al.* [30], which were performed on nominally undoped boule material with low micropipe density. Shortly before these earlier WMA measurements were made, there was another attempt to measure  $\Delta_{c1}$  in 4H-SiC from WMA measurements, but it was evidently hindered by poor quality of the available boule 4H-SiC [72]. It's not clear if the poor sample quality in that work induced excessive spectral broadening, but based on the relatively broad range of samples studied in the present work and in previous work [30], the width of the crystal-field split-off absorption onsets does not appear to be inherently limited by the quality of our samples.

It is therefore likely that the observed lifetime broadening here is due to intrinsic processes such as (a) phonon-mediated scattering of electrons (holes) to lower conduction band minima (higher valence band maxima) (note that both  $\Delta_{c1}$  and  $\Delta_{c2}$  lie within the range of energies susceptible to interband scattering by zone center phonons [19,21–24]) or (b) autoionization of the exciton through resonance with the continuum states of lower energy excitons. This latter interpretation agrees nicely with the observation that the transitions associated with the spin-orbit split-off exciton do not exhibit appreciable broadening, and the hydrogenic approximation of

40 meV for the fundamental gap exciton's binding energy exceeds the spin-orbit splitting  $\Delta'_{\text{so}}$ . If either interpretation is correct, it is not likely that the absorption onsets due to the crystal-field split-off valence band and second lowest conduction band can be further resolved using the method of WMA spectroscopy, since neither instrumental resolution nor crystal quality appear to be a limiting factor.

### IX. VALENCE BAND NONPARABOLICITY

In some, though not all, of the spin-orbit split pairs in the WMA spectrum, a small, broad bump appears between the two peaks. This can be seen most clearly in the spin-orbit split pairs due to the 52.3, 68.4, and 77.9 meV phonons, and to a lesser extent in the pairs due to the 50.4, 76.2, and 94.1 meV phonons (see Fig. 3). The shape of the bump is starkly different from the inverse-square-root dependence expected for indirect semiconductors with parabolic band extrema [56], although its shape and positioning between each pair of peaks appears to be fairly consistent, particularly for the former three phonons. In a previous study of the WMA spectrum in 4H-SiC, these were attributed to partial mixing between the  $\vec{E} \parallel \hat{c}$  and  $\vec{E} \perp \hat{c}$  polarizations [30].

Having re-examined the features at higher wavelength resolution, we were drawn to discount this claim due to the strong resemblance of the features with those that appear in the WMA spectra of the indirect semiconductors germanium (see Fig. 1 in Ref. [73]) and 3C-SiC (see the feature at 2.44 eV in Fig. 1 in Ref. [46] and Fig. 2 in Ref. [74]). In the case of germanium, the bump appears between a pair of LA phonon-assisted absorption onsets split by 1 meV, which is the splitting of the free exciton ground state due to electron mass anisotropy [73]. A calculation of germanium's exciton energy dispersion  $E(\vec{K})$  reveals that the pair of mass anisotropy split minima undergo an avoided crossing, which, in the energy interval between the two minima, produces a broad bump in the exciton density of states (and in turn, the absorption coefficient) between the two square-root-type van Hove singularities associated with the parabolic regions nearer to the minima [75,76].

Such a calculation has not yet been performed for 4H-SiC, although relativistic band structure calculations [16] show that a similar avoided crossing occurs in the  $\Gamma$ - $M$ - $K$  plane between the top two valence band maxima separated by the spin-orbit splitting. A few observations may be made to support the idea that this avoided crossing is responsible for the bumps observed in the WMA spectrum of 4H-SiC. The first is that, wherever the bumps do appear, they are consistently located between spin-orbit split, inverse-square-root-type absorption onsets associated with the valence band maxima. The second is that, in the hydrogenic model for the exciton [56], the exciton density of states is proportional to the exciton's total mass  $M = m_e + m_h$ . From this point of view, the curvature of the valence band should have a strong influence on the exciton density of states for  $m_h > m_e$ , which is generally true for each of the components of the effective mass tensors associated with the valence band maximum and conduction band minimum in 4H-SiC [58,77]. This argument is admittedly crude given that we are extrapolating the hydrogenic model to a case

in which it is clearly not applicable, but at this stage we only use this as a means to motivate further investigation.

Looking to other SiC polytypes for a moment, we note that the bump appearing in the WMA spectrum of 3C-SiC also appears between a spin-orbit split pair of inverse-square-root-type absorption onsets [46,74], and 3C-SiC exhibits an avoided crossing (along the  $\Lambda$  and  $\Sigma$  lines) between its spin-orbit split valence band maxima [16,74]. While the top-most valence band maxima of 6H SiC are more directly comparable to those of 4H-SiC, similar-looking features are notably absent from the WMA measurements of this polytype [72,74,78,79]. However, this may be attributed to the substantially higher electron effective mass along the  $M$ - $L$  line (which also exhibits substantial nonparabolicity of its own) [14,15,80,81], which, based on the arguments given above, may then exert a greater influence on the exciton density of states than the valence band effective mass and curvature.

The above reasoning was used in our previous work [47] to identify the origin of the bumps, but did not provide any quantitative evidence beyond that. For this work, we attempted to provide more substance to the idea by directly comparing the bumps in the measured WMA spectrum with the energy derivative  $dg_v/dE$  of the valence band density of states.  $dg_v/dE$  was obtained from the energy derivative of expression (3.10) used by Lehmann and Taut [82] to compute the density of states and the  $\vec{k} \cdot \vec{p}$  fit of Wellenhofer and Rössler to their (nonrelativistic) DFT band structure calculation for 4H-SiC [14]. A spin-orbit splitting parameter  $\Delta_2 = 3.5$  meV was chosen to reproduce the  $\sim 7$  meV spin-orbit splittings in the WMA spectrum. In Fig. 6, we show a comparison of  $g_v(E)$ , its energy derivative, and the spin-orbit splitting in the 52.3 meV phonon-assisted absorption onset. We see that while the top two valence band maxima both exhibit near-parabolic square-root-type contributions to  $g_v(E)$  within the first  $\sim 1$  meV below the maxima, there is a subtle departure from parabolicity in the energy region between the two maxima, which is further emphasized in the energy derivative. A comparison of  $dg_v/dE$  with the 52.3 meV phonon-assisted absorption onsets reveals slight differences (namely, the energy position of the bump's peak), although the qualitative similarity between the two is surprisingly good, given that no account was made for the electron-hole interaction or any possible energy dependence of the indirect transition matrix elements. A more detailed analysis which includes these effects might be able to add further clarity to the shape of these features as well as their absence in some of the observed spin-orbit split absorption onsets.

### X. EXCITON FINE STRUCTURE

As a result of the improved wavelength resolution ( $\delta\lambda \sim 0.1 \text{ \AA}$ ) obtained in the present WMA measurements, we have resolved a series of much smaller splittings than any of those described above. As shown in Fig. 7, we observe these splittings in both the  $\text{EX}_{\text{fg}}$  and  $\text{EX}_{\text{so}}$  components of the 40.2 meV phonon-assisted absorption onsets, the  $\text{EX}_{\text{so}}$  component of the 45.6 meV phonon-assisted absorption onset, and the  $\text{EX}_{\text{fg}}$  component of the 94.1 meV phonon-assisted absorption onset (this latter splitting had not been reported in our previous work [47], as it had not been completely resolved). Each of



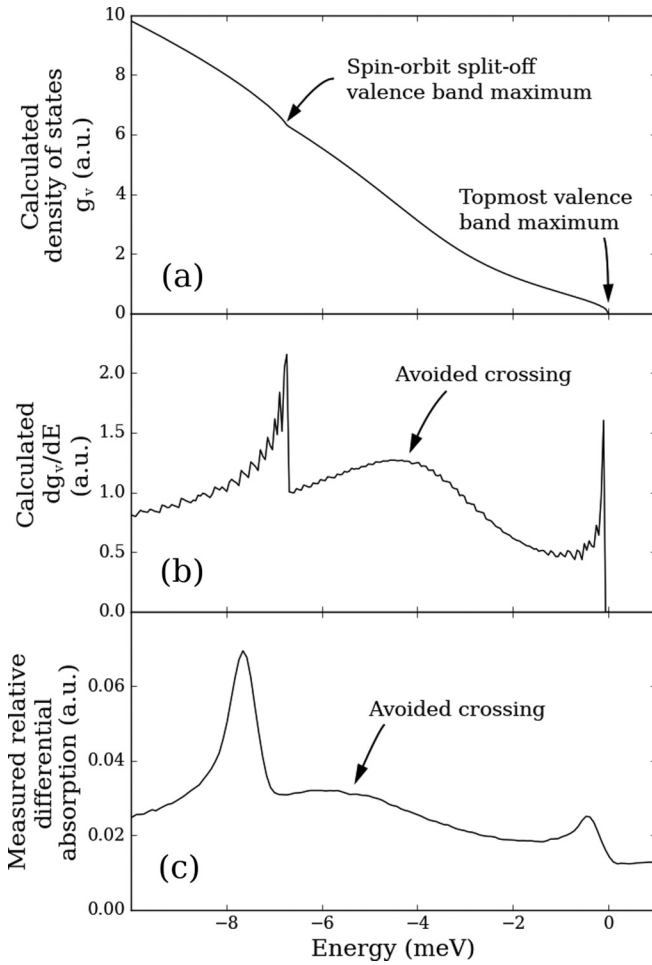


FIG. 6. (a) Density of states  $g_v(E)$  and (b) energy derivative of the density of states  $dg_v/dE$  in the first 10 meV below the topmost valence band maximum, calculated using  $\vec{k} \cdot \vec{p}$  parameters of Wellenhofer and Rössler [14]. The two topmost valence band maxima produce  $E^{1/2}$ - and  $E^{-1/2}$ -like onsets to  $g_v(E)$  and  $dg_v/dE$ , respectively, which are typical of parabolic band extrema and are separated by 7 meV (empirical spin-orbit splitting parameter supplied to the calculation and chosen to match experimental data). These two bands undergo an avoided crossing in the band structure, resulting in a “bump” in  $g_v(E)$  and  $dg_v/dE$  in the energy region between the two valence band maxima. In (c), an example of how the bump in the density of states results in a bump in between spin-orbit split absorption onsets in the wavelength-modulated absorption spectrum (in this case the transitions are assisted by the 52.3 meV phonon) is shown. Note that oscillations near the peaks in  $dg_v/dE$  are due to inaccuracies in the numerical calculation [82] of  $g_v(E)$  near van-Hove singularities, which may be reduced by the method of Methfessel *et al.* [83].

these splittings is  $0.7 \pm 0.1$  meV, and all have been observed to reproduce in samples cut from either of the two boules used (free standing epitaxial wafers were not measured in this wavelength range, as they were too thin to achieve reasonable sensitivity). Of note is the fact that all of these splittings appear in the WMA spectrum polarized  $\vec{E} \perp \hat{c}$ , whereas no such splittings are observed for the WMA spectrum polarized  $\vec{E} \parallel \hat{c}$ .

We attribute these splittings to a fourfold fine structure splitting in the ground states of both the fundamental gap

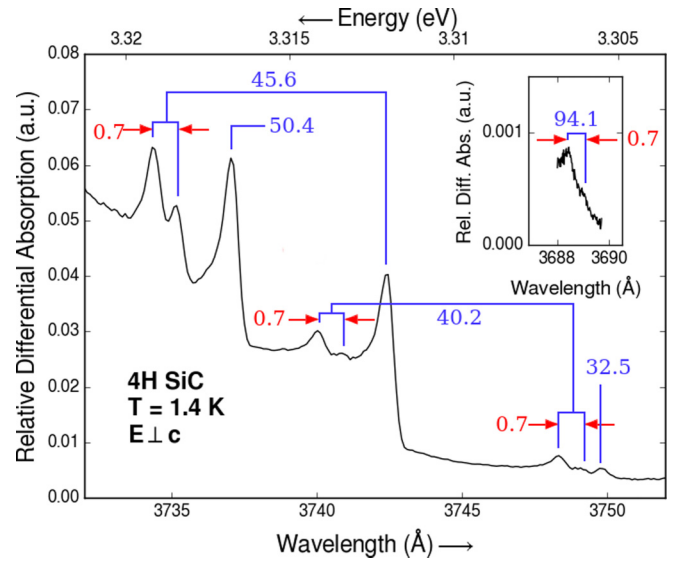


FIG. 7. Expanded view of the wavelength-modulated absorption measurements shown in Fig. 3(b). The peaks are labeled by the energy in meV of the principal phonon participating in the indirect transition. The 45.6 and 40.2 meV phonons give rise to a spin-orbit split pair with further,  $0.7 \pm 0.1$  meV splittings in either one or both of the spin-orbit split peaks. The inset shows an additional fine structure splitting of the same size for the 94.1 meV phonon (the corresponding spin-orbit split-off peak is not shown and did not exhibit any fine structure splitting). These splittings are due to a fourfold splitting in the free exciton ground state, which is in turn a result of electron mass anisotropy and electron-hole exchange interaction.

exciton  $EX_{fg}$  and the spin-orbit split-off exciton  $EX_{so}$ , which is due to electron mass anisotropy and electron-hole exchange interaction. In the following, we will show that this is consistent both with the multiplicity of the observed splittings and their occurrence only for  $\vec{E} \perp \hat{c}$ . To do so, we reconsider the selection rules for the creation of the fundamental gap exciton  $EX_{fg}$  but with electron spin now included. In this case, the irreducible representation for the hole wave function is  $\Gamma_9$  or  $\Gamma_7$  for the topmost or spin-orbit split-off valence band maximum, respectively [16], as described in Eq. (17). The electron wave function on the other hand transforms as the  $M_5$  representation of the  $C_{2v}$  group:

$$M_4 \otimes M_5 = M_5, \quad (20)$$

where, on the left,  $M_4$  describes the spatial component and  $M_5$  describes the spinor component. Combining the electron and hole wave functions together to form an exciton with a (fully symmetric) S-like envelope results in the following representations for the exciton:

$$\Gamma_9 \otimes M_5 = M_1 \oplus M_2 \oplus M_3 \oplus M_4, \quad (21)$$

where we have used the compatibility relation  $\Gamma_9 \rightarrow M_5$  between groups  $C_{6v}$  and  $C_{2v}$  [67]. Schematically, this result indicates that the free exciton ground state exhibits a splitting into four nondegenerate levels upon inclusion of spin for the electron and hole. It may also be shown that the very same result would follow for any free exciton composed of a hole at a  $\Gamma$  point valence band maximum and an electron at an

$M$  point conduction band minimum. In particular, this should also be true for the spin-orbit split-off exciton  $EX_{so}$ , and this is consistent with the observed fine structure splittings in some of the spin-orbit split-off components of the absorption onsets. In principal, the excitons  $EX_{cf}$  and  $EX_{c2}$  should also exhibit a fourfold splitting in their ground states, but because of the large spectral width of their associated features in the WMA spectrum, any fine structure is likely unobservable.

The nature of the splitting is somewhat analogous to that seen in atomic systems, in which combining two spin-1/2 electrons results in singlet and triplet states that are distinct in energy due to the exchange interaction. However, the  $C_{6v}$  point group symmetry associated with the  $\Gamma$  point would necessarily break the threefold degeneracy of the triplet state (with symmetry  $D_1^+$  of the full rotation group) into a singlet and doublet state:

$$D_1^+ \rightarrow \Gamma_2 \oplus \Gamma_5, \quad (22)$$

and the  $C_{2v}$  point group symmetry associated with the  $M$  point results in a further splitting of the doublet state:

$$\Gamma_2 \oplus \Gamma_5 \rightarrow M_3 \oplus (M_2 \oplus M_4). \quad (23)$$

This latter effect is the so-called mass anisotropy splitting, and is the result of a reduction in symmetry upon combining a hole with an electron occupying a lower symmetry point in the Brillouin zone. As for the singlet state (with symmetry  $D_0^+$  of the full rotation group), its symmetry reduces simply to  $M_1$  of the  $C_{2v}$  group, which completes the set of symmetry labels given in Eq. (21).

The relative contributions of electron-hole exchange and electron mass anisotropy to the observed splittings in this case are unknown, although in the case of silicon they were found to be comparable (up to a few tenths of a meV) [42]. We note that the size of the  $0.7 \pm 0.1$  meV splittings reported here for  $4H$ -SiC is similar to the mass anisotropy splittings measured in several other materials [40–46]. In particular, for  $3C$ -SiC, the mass anisotropy splitting is observed to be  $0.59 \pm 0.03$  meV in the TA phonon-assisted absorption onset [46].

An allowed transition to any one of the four exciton sublevels will occur if its symmetry representation is included in the direct product of the symmetry representations  $\Gamma_\omega$  and  $M_\Omega$  for the electron-photon and electron-phonon interactions. Depending on the phonon, the symmetry representation for the electron-phonon interaction can be any one of the single group representations  $M_1$  through  $M_4$ , whereas the symmetry representation for the electron-photon interaction will be the  $\Gamma_1$  or  $\Gamma_5$  representations of the  $C_{6v}$  group for  $\vec{E} \parallel \hat{c}$  or  $\vec{E} \perp \hat{c}$ , respectively. However, the result of this analysis shows that, for any given principal phonon, there is an allowed transition to any one or more of these sublevels for *both* polarizations of the incident light. This is clearly distinct from the selection rules for the case without electron spin, which predicted that  $M_1$  and  $M_3$  symmetry phonons participate only for  $\vec{E} \parallel \hat{c}$  and  $M_2$  and  $M_4$  symmetry phonons participate only for  $\vec{E} \perp \hat{c}$ , in agreement with the WMA and LTPL measurements.

In order to reconcile our measurements with the selection rules incorporating electron spin, we argue that, while they may be rigorously true, an allowed transition which is forbidden in the case without spin is simply too weak to be

TABLE IV. Multiplication table for the symmetry representations  $\Gamma_\omega$  and  $M_\Omega$  for the electron-photon and electron-phonon interactions, respectively. Representations labeled  $\Gamma$  are those of the  $C_{6v}$  group associated with the center of the Brillouin zone,  $\Gamma$ , and representations labeled  $M$  are from the  $C_{2v}$  group associated with the  $M$  point of the Brillouin zone. The results of those combinations which are consistent with the indirect transition selection rules [30] derived for the case without electron spin are shown in bold. We also use the compatibility relations  $\Gamma_1 \rightarrow M_1$  and  $\Gamma_5 \rightarrow M_2 \oplus M_4$  [67].

		$M_\Omega$			
		$M_1$	$M_2$	$M_3$	$M_4$
$\Gamma_\omega$	$\Gamma_1 (\vec{E} \parallel \hat{c})$	<b><math>M_1</math></b>	<b><math>M_2</math></b>	<b><math>M_3</math></b>	<b><math>M_4</math></b>
	$\Gamma_5 (\vec{E} \perp \hat{c})$	$M_2 \oplus M_4$	<b><math>M_1 \oplus M_3</math></b>	$M_2 \oplus M_4$	<b><math>M_1 \oplus M_3</math></b>

observed. In this case, we should consider only those combinations of  $\Gamma_\omega$  and  $M_\Omega$  which are consistent with the selection rules derived without spin. We summarize these in Table IV and represent them schematically in Fig. 8(a). From this, we can conclude that, despite the fourfold splitting of the free exciton energy levels, only two of the four sublevels, namely, the  $M_1$  and  $M_3$  symmetry sublevels, may ever be optically active. Furthermore, only one of these will be active for  $\vec{E} \parallel \hat{c}$  while both will be active for  $\vec{E} \perp \hat{c}$ . This is consistent with the observed twofold fine structure splittings, which are seen only in the  $\vec{E} \perp \hat{c}$  polarized WMA spectrum. For those absorption onsets in the  $\vec{E} \perp \hat{c}$  polarized WMA spectrum that do not exhibit fine structure splittings, the transition rates into one of the optically active sublevels must therefore be too small to observe.

This subtlety was alluded to in the preliminary group theory arguments we made previously [47] regarding the exciton fine structure, but has not been fully described until now. Another new, related insight which we have not discussed previously is that, while no fine structure splitting can be observed in the WMA spectrum polarized  $\vec{E} \parallel \hat{c}$ , there is an observable effect on the sizes of the measured spin-orbit splittings  $\Delta'_{so}$ . From the selection rules described in Table IV and the diagram in Fig. 8(b), we find that for an  $M_1$  symmetry phonon,  $\Delta'_{so}$  should be equal to the energy separation between the  $M_1$  sublevels of the fundamental gap and spin-orbit split-off excitons, whereas for an  $M_3$  symmetry phonon,  $\Delta'_{so}$  should be equal to the energy separation between their  $M_3$  sublevels.  $\Delta'_{so}$  may be different for these two cases if one or both of the following conditions are true: the  $M_1$ - $M_3$  sublevel separation is different for the two excitons or the sublevel energetic ordering is reversed between the two excitons. If we now group the measured values for  $\Delta'_{so}$  according to the symmetry of the corresponding phonon (given in Table I), we find that for  $M_1$  symmetry phonons,  $\Delta'_{so}{}^{(1)} = 7.2 \pm 0.2$  meV, and for  $M_3$  symmetry phonons,  $\Delta'_{so}{}^{(3)} = 6.7 \pm 0.2$  meV. This observed bifurcation in the measured spin-orbit splittings is therefore the dominant contributor to the  $\pm 0.6$  meV measurement uncertainty given earlier in Sec. V and in previous WMA measurements of  $4H$ -SiC [30], where phonon symmetry was not distinguished. While there is a much weaker correlation between  $\Delta'_{so}$  and the phonon symmetry for  $\vec{E} \perp \hat{c}$ , a fine

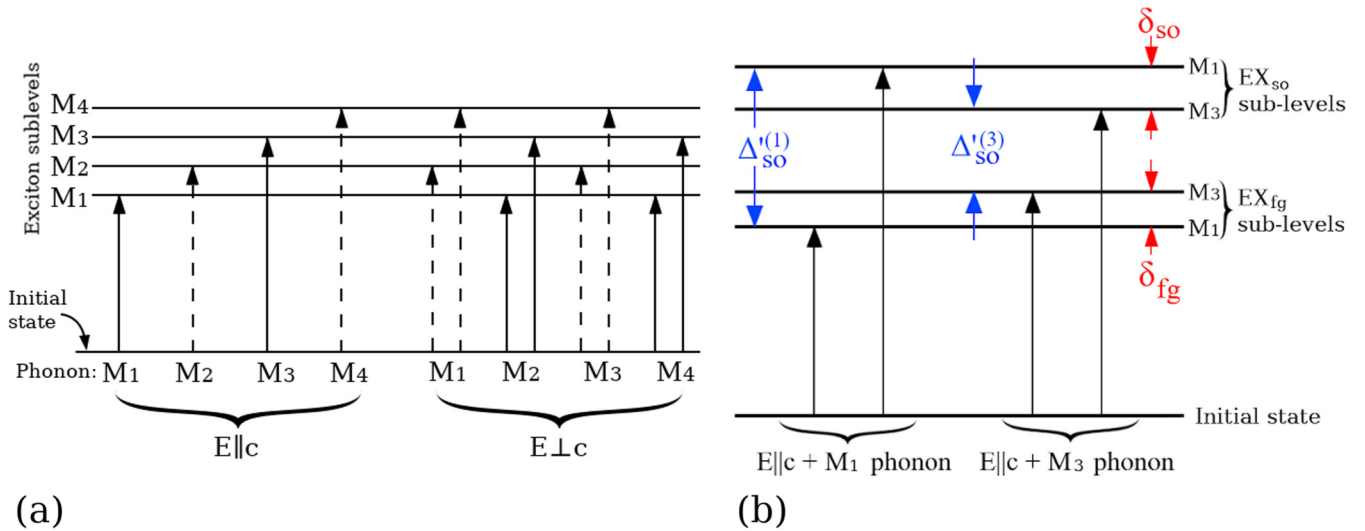


FIG. 8. (a) Schematic representation of the selection rules for free indirect exciton absorption with electron and hole spin included. Solid arrows indicate allowed transitions into a particular sublevel of the free exciton ground state (shown in arbitrary ordering and with symmetries  $M_1$  through  $M_4$  of the  $C_{2v}$  group) and emission of a phonon with the indicated symmetry (also from the  $C_{2v}$  group). Dashed arrows indicate presumably weak transitions which are allowed with electron and hole spins included in the group theory analysis, but are forbidden when spin is not included. In (b) is shown a similar diagram but with sublevels of the spin-orbit split-off exciton ( $EX_{so}$ ) in addition to those of the fundamental gap exciton ( $EX_{fg}$ ) (only the  $M_1$  and  $M_3$  sublevels associated with the “strong” transitions in (a) are shown). Due to the selection rules shown in (a) (which apply to both  $EX_{fg}$  and  $EX_{so}$ ), if the energetic ordering of the  $M_1$  and  $M_3$  sublevels is reversed between the  $EX_{fg}$  and  $EX_{so}$  excitons, a different spin-orbit splitting ( $\Delta'_{so}{}^{(1)}$  or  $\Delta'_{so}{}^{(3)}$ ) will be observed for  $\vec{E} \parallel \hat{c}$  depending on whether the  $M_1$  or  $M_3$  symmetry exciton sublevel is active (or alternatively: whether an  $M_1$  or  $M_3$  symmetry phonon is emitted). This would also be the case if the ordering were the same, but the fine structure splittings  $\delta_{fg}$  and  $\delta_{so}$  between the  $M_1$  and  $M_3$  sublevels of  $EX_{fg}$  and  $EX_{so}$  were different.

structure splitting is not observed in all absorption onsets in this polarization despite there being two optically active sublevels, and so in this case it is ambiguous as to which pairs of sublevels correspond to the measured energy separation  $\Delta'_{so}$  (if one or more of the two peaks in a given spin-orbit split absorption onset exhibit fine structure, we invariably measure  $\Delta'_{so}$  from the lower energy peak within the fine structure splitting).

Given that not all of the 24 principal phonons have been identified in our WMA measurements, there is a possibility that one of the observed peaks within a given fine structure splitting is due to one of the four principal phonons which has not yet been accounted for in our listing in Table I. However, from a comparison with the majority of the calculated phonon dispersion relations in  $4H$ -SiC [18–24], all of the lower energy principal phonons (i.e. those below the phonon energy gap between roughly 80 and 90 meV) have been accounted for, and with the exception of the 94.1 meV principal phonon, these are the principal phonons that exhibit fine structure splittings. Furthermore, should a given fine structure splitting be due to a pair of near-degenerate principal phonons, this splitting should also be observed in the LTPL spectrum. The fact that these splittings were not observed in the LTPL supports our original conclusion, since in this case the  $\sim 0.7$  meV separation between sublevels is too large to observe recombination from the upper sublevel at 2 K ( $k_B T = 0.2$  meV).

## XI. CONCLUSION

As with many other semiconductors and insulators, the measurement of the fundamental absorption edge in silicon

carbide may provide direct insight into the size of the band gap and nature of the electronic states nearest to the band extrema, which are the most relevant to the operation of silicon carbide-based devices. However, due to the indirect nature of the gap and large number of momentum-conserving phonons in  $4H$ -SiC, many distinct indirect absorption processes are possible within a very narrow wavelength region of the absorption spectrum, making it difficult to clearly identify the valence and conduction band extrema between which the transitions occur. We have largely overcome this challenge by measuring the wavelength-modulated absorption spectrum of high-purity  $4H$ -SiC near its fundamental edge at substantially higher wavelength resolution ( $\delta\lambda < 0.1$  Å) than that of previous studies. Over the 3450–3760 Å range of measurements, we have resolved 49 distinct onsets of absorption which are reproducible in all samples and whose shapes are each characteristic of free indirect exciton absorption. By comparing these measurements to high-resolution low-temperature photoluminescence measurements of the same samples, we have determined the phonon energies of 20 of the 24 principal phonon modes in  $4H$ -SiC and identified all 49 features in the wavelength-modulated absorption spectrum as indirect transitions between one of the three highest valence band maxima at  $\Gamma$  to one of the two lowest conduction band minima at  $M$ .

The energy separations between these valence and conduction band extrema are associated with the measured splittings  $\Delta'_{so} = 7.0 \pm 0.6$  meV,  $\Delta'_{cf} = 56 \pm 3$  meV, and  $\Delta'_{c2} = 136 \pm 3$  meV (respectively, the spin-orbit splitting, crystal-field splitting, and conduction band splitting) in the observed absorption onsets, which generally fall within the broad range of results from band structure calculations and other experiments. The

precision with which the crystal-field splitting  $\Delta'_{cf}$  and conduction band minimum splitting  $\Delta'_{c2}$  have been determined is evidently limited by intrinsic lifetime broadening of the free exciton associated with the corresponding band extrema. A more precise determination of these band parameters will require further confirmation from independent experimental techniques, which, to date, are relatively few despite the obvious importance of these parameters to the modeling of high-temperature and high-voltage devices.

Further detail has also been resolved in the previously anomalous “bumps” between spin-orbit split pairs of absorption onsets in the wavelength-modulated absorption spectrum, which has allowed us to associate them with the nonparabolic dispersion near the valence band maximum. We have also resolved several additional splittings of a much smaller scale,  $0.7 \pm 0.1$  meV, which relate to a fine structure splitting in the free exciton ground state due to electron mass anisotropy and the electron-hole exchange interaction. Such splittings have been observed in the absorption spectra of other semiconductors [40–46], but never before in the absorption spectrum of 4H-SiC. It should be possible to observe these splittings in the high-resolution LTPL of 4H-SiC at elevated temperatures (such that  $k_B T \approx 0.7$  meV), as has been done in other materials [41,46,84].

These results underscore the rather direct relationship between measurements of the fundamental absorption edge and the detailed properties of the electronic band structure relative to other experimental techniques, although a fully rigorous comparison would require a theoretical treatment of the free exciton in 4H-SiC which incorporates both the anisotropy

and nonparabolicity of the band extrema. Some possible extensions to our experimental work include measuring the LTPL spectrum of 4H-SiC at elevated temperatures, as mentioned previously, as well as the measurement of the absorption edge in 4H-SiC under applied uniaxial stress or static magnetic fields, which have been used in semiconductors of the diamond and zincblende crystal structures to estimate the strengths (both relative and absolute) of electron-phonon and hole-phonon interaction [69–71] or to separate out degenerate components of the exciton energy level structure [43,85,86]. Despite their complicated structure, the fundamental absorption edge, low-temperature photoluminescence spectrum, and the indirect transitions that characterize them in 4H-SiC are just now becoming accessible to first principles calculations with unprecedented detail. Nevertheless, there do remain some lingering discrepancies between theory and experiment, particularly in relation to the experimental observation that lower energy principal phonons (with  $\hbar\Omega < 55$  meV) are associated with significantly lower indirect transition rates than that of higher energy principal phonons, which was not found in the first principles calculation of the LTPL spectrum [18].

#### ACKNOWLEDGMENTS

We thank the II-VI Foundation for their continual support of this work; Al Burk of Wolfspeed for generously providing us with the boule material used in these measurements; and Daniel Yates, Charlie Tabachnick, Gabriel Freedman, and Josh Lascek for polishing of samples.

- 
- [1] O. Weigel, *Nachr. Ges. Wiss.*, 264 (1915).
  - [2] W. J. Choyke, L. Patrick, and D. R. Hamilton, in *Proceedings of the International Conference on the Physics of Semiconductors* (Academic, Paris, France, 1964), p. 751.
  - [3] W. J. Choyke and L. Patrick, *Phys. Rev.* **105**, 1721 (1957).
  - [4] L. Patrick and W. J. Choyke, *Phys. Rev.* **186**, 775 (1969).
  - [5] W. J. Choyke and L. Patrick, *Phys. Rev.* **127**, 1868 (1962).
  - [6] L. Patrick, D. R. Hamilton, and W. J. Choyke, *Phys. Rev.* **132**, 2023 (1963).
  - [7] D. R. Hamilton, L. Patrick, and W. J. Choyke, *Phys. Rev.* **138**, A1472 (1965).
  - [8] H. R. Philipp, *Phys. Rev.* **111**, 440 (1958).
  - [9] J. Bardeen, L. H. Hall, and F. J. Blatt, in *Photoconductivity Conference*, edited by R. G. Breckenridge, B. R. Russell, and E. E. Hahn (Wiley, New York, USA, 1954), p. 146.
  - [10] J. A. Lely, *Ber. Dtsch. Keram. Ges.* **32**, 229 (1955).
  - [11] P. Käckell, B. Wenzien and F. Bechstedt, *Phys. Rev. B* **50**, 10761 (1994).
  - [12] G. L. Zhao and D. Bagayoko, *New J. Phys.* **2**, 16 (2000).
  - [13] C. H. Park, B.-H. Cheong, K.-H. Lee, and K. J. Chang, *Phys. Rev. B* **49**, 4485 (1994).
  - [14] G. Wellenhofer and U. Rössler, *Phys. Status Solidi B* **202**, 107 (1997).
  - [15] W. R. L. Lambrecht, S. Limpijumnong, S. N. Rashkeev, and B. Segall, *Phys. Status Solidi B* **202**, 5 (1997).
  - [16] C. Persson and U. Lindefelt, *J. Appl. Phys.* **82**, 5496 (1997).
  - [17] G. Pennington and N. Goldsman, *Phys. Rev. B* **64**, 045104 (2001).
  - [18] S. Lyu and W. R. L. Lambrecht, *Phys. Rev. B* **101**, 045203 (2020).
  - [19] N. H. Protik, A. Katre, L. Lindsay, J. Carrete, N. Mingo, and D. Broido, *Mater. Today Phys.* **1**, 31 (2017).
  - [20] J. Serrano, J. Strempler, M. Cardona, M. Schwoerer-Böhning, H. Requardt, M. Lorenzen, B. Stojetz, P. Pavone, and W. J. Choyke, *Mater. Sci. Forum* **443-436**, 257 (2003).
  - [21] D. Strauch, B. Dorner, A. A. Ivanov, M. Krisch, J. Serrano, A. Bosak, W. J. Choyke, B. Stojetz, and M. Malorny, *Mater. Sci. Forum* **527-529**, 689 (2006).
  - [22] K. Karch, P. Pavone, W. Windl, O. Schütt, and D. Strauch, *Phys. Rev. B* **50**, 17054 (1994).
  - [23] M. Hofmann, A. Zywietz, K. Karch, and F. Bechstedt, *Phys. Rev. B* **50**, 13401 (1994).
  - [24] I. G. Ivanov, U. Lindefelt, A. Henry, O. Kordina, C. Hallin, M. Aroyo, T. Egilsson, and E. E. Janzén, *Phys. Rev. B* **58**, 13634 (1998).
  - [25] J. Pernot, W. Zawadzki, S. Contreras, J. L. Robert, E. Neyret, and L. Di Cioccio, *J. Appl. Phys.* **90**, 1869 (2001).



- [26] E. Bellotti, H.-E. Nilsson, K. F. Brennan, P. P. Ruden, and R. Trew, *J. Appl. Phys.* **87**, 3864 (2000).
- [27] H.-E. Nilsson, E. Bellotti, K. F. Brennan, and M. Hjelm, *Mater. Sci. Forum* **338–342**, 765 (2000).
- [28] M. Hjelm, H.-E. Nilsson, A. Martinez, K. F. Brennan, and E. Bellotti, *J. Appl. Phys.* **93**, 1099 (2003).
- [29] A.-B. Chen and P. Srichaikul, *Phys. Status Solidi B* **202**, 81 (1997).
- [30] S. G. Sridhara, S. Bai, O. Shigiltchhoff, R. P. Devaty, and W. J. Choyke, *Mater. Sci. Forum* **338–342**, 567 (2000).
- [31] W. M. Klahold, C. Tabachnick, G. Freedman, R. P. Devaty, and W. J. Choyke, *Mater. Sci. Forum* **897**, 250 (2017).
- [32] P. Grivickas, V. Grivickas, J. Linnros, and A. Galeckas, *J. Appl. Phys.* **101**, 123521 (2007).
- [33] P. Grivickas, K. Redeckas, K. Gulbinas, A. M. Conway, L. F. Voss, M. Bora, S. Sampayan, M. Vengris, and V. Grivickas, *J. Appl. Phys.* **125**, 225701 (2019).
- [34] S. Lyu and W. R. L. Lambrecht, *Phys. Rev. B* **102**, 079904(E) (2020).
- [35] G. B. Dubrovskii and V. I. Sankin, *Fiz. Tverd. Tela* **17**, 2776 (1975) [*Sov. Phys. Solid State* **17**, 1847 (1975)].
- [36] I. Shalish, I. B. Altfeder, and V. Narayanamurti, *Phys. Rev. B* **65**, 073104 (2002).
- [37] Y. Ding, K.-B. Park, J. P. Pelz, A. V. Los, and M. S. Mazzola, *Mater. Sci. Forum* **457–460**, 1077 (2004).
- [38] B. Kaczer, H.-J. Im, J. P. Pelz, J. Chen, and W. J. Choyke, *Phys. Rev. B* **57**, 4027 (1998).
- [39] F. Fabbri, D. Cavalcoli, and A. Cavallini, *Acta Materialia* **60**, 3350 (2012).
- [40] S. Zwerdling, L. Roth, and B. Lax, *J. Phys. Chem. Solids* **8**, 397 (1959).
- [41] M. L. W. Thewalt and R. R. Parsons, *Solid State Commun.* **20**, 97 (1976).
- [42] D. Labrie, M. L. W. Thewalt, I. J. Booth, and G. Kirczenow, *Phys. Rev. Lett.* **61**, 1882 (1988).
- [43] J. Halpern and B. Lax, *J. Phys. Chem. Solids* **27**, 111 (1966).
- [44] T. Nishino, M. Takeda, and Y. Hamakawa, *J. Phys. Soc. Jpn.* **37**, 1016 (1974).
- [45] R. G. Humphreys, U. Rössler, and M. Cardona, *Phys. Rev. B* **18**, 5590 (1978).
- [46] I. S. Gorban', V. A. Gubanov, V. G. Lysenko, A. A. Pletyushkin, and V. B. Timofeev, *Fiz. Tverd. Tela* **26**, 2282 (1984) [*Sov. Phys. Solid State* **26**, 1385 (1984)].
- [47] W. M. Klahold, W. J. Choyke, and R. P. Devaty, *Mater. Sci. Forum* **924**, 239 (2018).
- [48] B. Batz, *Solid State Commun.* **5**, 985 (1967).
- [49] B. Batz, *Semicond. Semimet.* **9**, 327 (1972).
- [50] K. L. Shaklee and J. E. Rowe, *Appl. Opt.* **9**, 627 (1970).
- [51] M. Cardona, *Modulation Spectroscopy* (Academic, New York, 1969), pp. 108–109.
- [52] F. G. Brickwedde, H. van Dijk, M. Durieux, J. R. Clement, and J. K. Logan, *J. Research Natl. Bur. Standards* **64A**, 1 (1960).
- [53] S. G. Sridhara, T. J. Eperjesi, R. P. Devaty, and W. J. Choyke, *Mater. Sci. Eng.: B* **61–62**, 229 (1999).
- [54] I. G. Ivanov, C. Hallin, A. Henry, O. Kordina, and E. Janzén, *J. Appl. Phys.* **80**, 3504 (1996).
- [55] E. R. Glaser, B. V. Shanabrook, and W. E. Carlos, *Appl. Phys. Lett.* **86**, 052109 (2005).
- [56] R. J. Elliott, *Phys. Rev.* **108**, 1384 (1957).
- [57] D. Volm, B. K. Meyer, D. M. Hofmann, W. M. Chen, N. T. Son, C. Persson, U. Lindefelt, O. Kordina, E. Sörman, A. O. Konstantinov, B. Monemar, and E. Janzén, *Phys. Rev. B* **53**, 15409 (1996).
- [58] N. T. Son, P. N. Hai, W. M. Chen, C. Hallin, B. Monemar, and E. Janzén, *Phys. Rev. B* **61**, R10544 (2000).
- [59] L. Patrick and W. J. Choyke, *Phys. Rev. B* **2**, 2255 (1970).
- [60] K. L. Shaklee and R. E. Nahory, *Phys. Rev. Lett.* **24**, 942 (1970).
- [61] W. J. Choyke, R. P. Devaty, L. L. Clemen, M. F. MacMillan, M. Yoganathan, and G. Pensl, *Inst. Phys. Conf. Ser.* **142**, 257 (1996).
- [62] W. J. Choyke, *Mater. Res. Bull.* **4**, S141 (1969).
- [63] H. Dai, M. A. Gundersen, C. W. Myles, and P. G. Snyder, *Phys. Rev. B* **37**, 1205 (1988).
- [64] D. G. Thomas and J. J. Hopfield, *Phys. Rev.* **150**, 680 (1966).
- [65] I. S. Gorban', A. P. Krokhmal', V. I. Levin, A. S. Skirda, Yu. M. Tairov, and V. F. Tsvetkov, *Fiz. Tekn. Poloprovdn.* **21**, 194 (1987) [*Sov. Phys. Semicond.* **21**, 119 (1987)].
- [66] G. Davies, *J. Phys. Chem. Solids* **31**, 883 (1970).
- [67] G. G. Koster, J. O. Dimmock, R. G. Wheeler, and H. Statz, *Properties of the 32 Point Groups* (MIT Press, Cambridge, 1963).
- [68] M. L. Cohen and S. G. Louie, *Fundamentals of Condensed Matter Physics* (Cambridge University Press, Cambridge, 2016), p. 222.
- [69] J.-C. Merle, M. Capizzi, P. Fiorini, and A. Frova, *Phys. Rev. B* **17**, 4821 (1978).
- [70] F. H. Pollak, A. Feldblum, H. D. Park, and P. E. Vanier, *Solid State Commun.* **28**, 161 (1978).
- [71] O. J. Glembocki and F. H. Pollak, *Phys. Rev. B* **25**, 1193 (1982).
- [72] W. J. Choyke, R. P. Devaty, and S. G. Sridhara, *Phys. Scr.* **T79**, 9 (1999).
- [73] A. Frova, G. A. Thomas, R. E. Miller, and E. O. Kane, *Phys. Rev. Lett.* **34**, 1572 (1975).
- [74] R. G. Humphreys, D. Bimberg, and W. J. Choyke, *Solid State Commun.* **39**, 163 (1981).
- [75] E. O. Kane, *Phys. Rev. B* **11**, 3850 (1975).
- [76] M. Altarelli and N. O. Lipari, *Phys. Rev. Lett.* **36**, 619 (1976).
- [77] N. T. Son, W. M. Chen, O. Kordina, A. O. Konstantinov, B. Monemar, and E. Janzén, *Appl. Phys. Lett.* **66**, 1074 (1995).
- [78] R. P. Devaty, W. J. Choyke, S. G. Sridhara, L. L. Clemen, D. G. Nizhner, D. J. Larkin, T. Troffer, G. Pensl, T. Kimoto, and H. S. Kong, *Mater. Sci. Forum* **264–268**, 455 (1998).
- [79] W. M. Klahold, W. J. Choyke, and R. P. Devaty, *Mater. Sci. Forum* **963**, 341 (2019).
- [80] N. T. Son, O. Kordina, A. O. Konstantinov, W. M. Chen, E. Sörman, B. Monemar, and E. Janzén, *Appl. Phys. Lett.* **65**, 3209 (1994).
- [81] C. Persson and U. Lindefelt, *Phys. Rev. B* **54**, 10257 (1996).
- [82] G. Lehmann and M. Taut, *Phys. Status Solidi B* **54**, 469 (1972).
- [83] M. S. Methfessel, M. H. Boon, and F. M. Mueller, *J. Phys. C* **16**, L949 (1983).
- [84] Y. Hazama, N. Naka, and H. Stolz, *Phys. Rev. B* **90**, 045209 (2014).
- [85] J. Donecker and J. Kluge, *Phys. Status Solidi B* **81**, 199 (1977).
- [86] S. Zwerdling, B. Lax, L. M. Roth, and K. J. Button, *Phys. Rev.* **114**, 80 (1959).